



HAL
open science

Multi-step limit cycle generation for Rabbit's walking based on nonlinear low dimensional predictive control scheme

Ahmed Chemori, Mazen Alamir

► **To cite this version:**

Ahmed Chemori, Mazen Alamir. Multi-step limit cycle generation for Rabbit's walking based on nonlinear low dimensional predictive control scheme. *Mechatronics*, 2006, 16 (5), pp.259-277. 10.1016/j.mechatronics.2005.12.001 . hal-00083873

HAL Id: hal-00083873

<https://hal.science/hal-00083873>

Submitted on 27 Nov 2006

HAL is a multi-disciplinary open access archive for the deposit and dissemination of scientific research documents, whether they are published or not. The documents may come from teaching and research institutions in France or abroad, or from public or private research centers.

L'archive ouverte pluridisciplinaire **HAL**, est destinée au dépôt et à la diffusion de documents scientifiques de niveau recherche, publiés ou non, émanant des établissements d'enseignement et de recherche français ou étrangers, des laboratoires publics ou privés.



ELSEVIER

Available online at www.sciencedirect.com

SCIENCE @ DIRECT®

Mechatronics xxx (2006) xxx–xxx

MECHATRONICS

Multi-step limit cycle generation for Rabbit's walking based on a nonlinear low dimensional predictive control scheme

Ahmed Chemori *, Mazen Alamir

Laboratoire d'Automatique de Grenoble, UMR 5528, BP46, Domaine Universitaire, 38400 Saint Martin d'Hères, France

Received 22 February 2005; accepted 7 December 2005

8 Abstract

In this paper, a new nonlinear predictive control scheme is proposed for a five-link planar under-actuated biped walking robot. The basic feature in the proposed strategy is to use on-line optimization to update the tracked trajectories in the completely controlled variables (actuated coordinates) in order to enhance the behavior and the stability of the remaining indirectly controlled ones (unactuated coordinates). The stability issue is discussed using the Poincaré's section tool leading to a computable criterion that enables the stability of the overall scheme to be investigated as well as the computation of a candidate region of attraction. The whole framework is illustrated through simulation case-studies. To attest the efficiency of the proposed scheme, robustness against model uncertainties and ground irregularities are investigated by simulation studies.

© 2006 Elsevier Ltd. All rights reserved.

Keywords: Biped robots; Dynamic walking; Multi-step limit cycle; Nonlinear optimization; Nonlinear predictive control; Orbital stability

18 Résumé

Dans cet article une nouvelle approche de commande prédictive non linéaire est proposée pour un robot marcheur bipède à cinq segments sous actionné. La caractéristique principale dans la stratégie proposée est d'utiliser l'optimisation en-ligne pour mettre à jour les trajectoires à poursuivre sur les variables complètement commandables (coordonnées actionnées) dans le but d'améliorer le comportement et la stabilité des variables indirectement commandées (coordonnées non actionnées). La stabilité est analysée par un outil graphique basé sur la section de Poincaré. Ceci permet, en plus de l'analyse la stabilité du système en boucle fermée, d'estimer la région d'attraction. L'approche proposée est illustrée à travers différents scénarios de simulations. La robustesse, quant à elle, est analysée par rapport à des incertitudes dans le modèle du robot, et des irrégularités dans le sol.

© 2006 Elsevier Ltd. All rights reserved.

Mots-clés: Robots bipèdes; Marche dynamique; Cycle limite d'ordre multiple; Optimisation non linéaire; Commande prédictive non linéaire; Stabilité orbitale

30 1. Introduction

In recent years, the robotics community has shown increasing interest in the area of legged walking robots

[29,2]. An excellent database of climbing and walking robots built all over the world can be found in [2]. One of the serious reasons for exploring the use of legged robots is the mobility [23], there is a need for vehicles that can travel in difficult terrains, where existing wheeled vehicles cannot go, since wheels excel on prepared surfaces such as rails and roads, but they perform poorly on rough terrains. Moreover, walking robots could co-exist with their

* Corresponding author.

E-mail addresses: Ahmed.Chemori@inpg.fr (A. Chemori), Mazen.Alamir@inpg.fr (M. Alamir).

41 creators without any costly modification to the environ-
42 ment created for humans.

43 In walking locomotion [23], two gaits could be under-
44 lined. *Static walking* which refers to a system which stays
45 balanced by always keeping the center of mass (c.o.m.) of
46 the system vertically projected over the polygon of support
47 formed by feet. On the contrary, *dynamic walking*
48 [24,21,13,22] is not constrained in such a manner, therefore
49 the c.o.m. may leave the support polygon for periods of
50 time. Biped robots [23,34,24] have high mobility that
51 allows them to achieve *dynamic walking*, consequently high
52 speeds could be reached due to the horizontal acceleration.

53 Currently, many research groups in the world are work-
54 ing on biped robots, either on optimization of leg and foot
55 trajectory, stable walking control, or hardware design. The
56 main thrust of current research on biped control includes
57 many proposed control approaches, such as intuitive con-
58 trol [28], intelligent learning control [19], neural network
59 control [18], passivity based control [33], sliding control
60 [6], impedance control [25], optimal control [14], computed
61 torque control [5], and tracking control [31,30].

62 From a control viewpoint, the major academic interest
63 of bipeds comes from (1) their hybrid nature resulting from
64 the unavoidable impacts [3] with the ground which can pro-
65 duce discontinuities (jumps) in the generalized velocities.
66 (2) Another interesting point is under-actuation, indeed
67 biped walking robots may be under-actuated (case of Rab-
68 bit) that is the robot has fewer number of actuators than
69 the number of degrees of freedom. The way this under-
70 actuation is handled may be used to give a particularly
71 clear insight into the set of solutions proposed so far within
72 the academic control community.

73 1. One way to overcome the under-actuation related-diffi-
74 culty is to define virtual controls [8]. Typically, reference
75 trajectories are defined on the whole state including indi-
76 rectly controlled sub-states. These trajectories are depen-
77 dent on some parameter vector p that can be either a
78 virtual time, a remaining free polynomial coefficient or
79 both. Generally, the second time-derivative of the param-
80 eter p becomes a virtual additional control enabling
81 under-actuation to be conceptually overcome. Clearly,
82 technical details are to be investigated when this second
83 derivative is monitored by the tracking requirements (vir-
84 tual time needs to be monotonic, coefficient excursions
85 have to be compatible with geometric constraints, etc.)
86 The reference trajectories to be tracked may be computed
87 using classical constrained optimal control tools. Several
88 optimization criterions have been proposed [31,26,30].
89 2. A second way to handle under-actuation is to use the
90 concept of virtual constraints and the associated zero-
91 dynamics [12,35,36]. Namely, some regulated output is
92 suitably defined that can be exactly tracked using the
93 available control inputs. The constrained dynamics of
94 the remaining sub-state on the zero-output manifold is
95 then called the zero-dynamics [17]. This methodology
96 is therefore based on the analytical study of the resulting

zero-dynamics that corresponds to each particular 97
choice of the regulated output. If the latter is taken in 98
a parameterized closed-loop form, off-line optimization 99
can then be used to enhance the asymptotic stability of 100
the zero-dynamics [12,35,36]. A particular feature when 101
dealing with the zero-dynamics associated to bipeds is 102
their hybrid nature [36]. 103

3. A third way to handle under-actuation in nonlinear 104
dynamical systems is predictive control schemes 105
[4,20,11]. Indeed, these schemes ensure stability by con- 106
trolling the behavior of the whole state at some future 107
time, say N -sampling times ahead. This naturally sup- 108
presses under-actuation since the number of control 109
d.o.f. is $r \times N$ where r is the number of actuators while 110
the controlled state is still n -dimensional. Therefore, 111
under-actuation generically *disappears* as soon as 112
 $Nr \geq n$. 113
114

The work proposed in this paper might be viewed as a 115
mixture of the last two categories. Namely a nonlinear pre- 116
dictive control scheme is proposed for the control of a five- 117
link 7 d.o.f. under-actuated biped robot while the stability 118
of the resulting zero-dynamics is explicitly studied. Con- 119
trary to the approach adopted in [1], where a somehow 120
black-box formulation is used to define the auxiliary 121
open-loop optimization problem, our approach leads to 122
low dimensional decision variables. This may be crucial 123
in a real-time implementation context. In particular, it is 124
shown that with a scalar such open-loop optimization 125
problem, provably stable and quasi-cyclic motions can be 126
generated. 127

The basic differences between the approach proposed in 128
this paper and existing provably stable limit-cycle genera- 129
tion can be summarized as follows: 130

- The limit cycle so-obtained may include several steps. 131
Namely, the robot configuration just after the impact 132
is not necessarily the same as the one just after the pre- 133
ceding impact. This happens especially with very low 134
dimensional (scalar) predictive control. By increasing 135
the d.o.f. of the control parameterization, classical 136
one-step limit cycles may be recovered, but the underly- 137
ing predictive control may not be real-time 138
implementable. 139
- The resulting closed-loop trajectories do not necessarily 140
correspond to a periodic motion of the torso. The latter 141
converges to a neighborhood of a stable limit cycle. This 142
is a crucial point since it has been pointed out in [27,9] 143
that such periodic motion is hard to achieve with at least 144
polynomial trajectories of the actuated variables. 145
146

Sufficient conditions for the stability of the feedback 147
scheme are derived together with a concrete computation 148
procedure to compute the corresponding region of attrac- 149
tion related to the zero-dynamics of the closed-loop sys- 150
tem. 151

152 This paper is organized as follows. First, the biped robot
 153 prototype is described in Section 2. Then the proposed pre-
 154 dictive control approach is presented in a rather general
 155 setting (Section 3). Computable sufficient conditions for
 156 stability are derived and implementation related topics
 157 are discussed in Section 4. Finally simulation results are
 158 given in Section 5, illustrating the potentiality of the pro-
 159 posed solution. These simulations include scenarios where
 160 a stable walk is obtained from the rest position as well as
 161 transitions between different desired mean walking speeds.
 162 Robustness against model parameters uncertainties and
 163 ground irregularities are also verified. The paper ends by
 164 some concluding remarks.

165 2. The RABBIT prototype description

166 The academic prototype RABBIT [10] is a biped walking
 167 robot with five links and seven d.o.f. (see Fig. 1), which
 168 results from the joint effort of several French laboratories
 169 (Mechanical engineering, Automatic control, and Robot-
 170 ics) working on a project on control of walking robots.¹
 171 By means of guidance device, RABBIT walks in a circular
 172 path (see Fig. 2) while looking like a planar biped. The
 173 counter-balance should be used to offset the weight of the
 174 lateral stabilization bar in the guidance device. More tech-
 175 nical details about the testbed can be found in [10].

176 2.1. Dynamic model

177 Using Lagrange formulation [32], the mathematical
 178 model describing the biped moving in the sagittal plane is
 179 as follows:
 180

$$182 M(q)\ddot{q} + N(q, \dot{q})\dot{q} + G(q) = Su + F_{\text{ext}} \quad (1)$$

183 where $M(q) \in \mathbb{R}^{7 \times 7}$ is the inertia matrix, $N(q, \dot{q}) \in \mathbb{R}^{7 \times 7}$ con-
 184 tains the centrifugal and Coriolis forces terms, $G(q) \in \mathbb{R}^7$ is
 185 the vector of gravitational forces, $u = [u_1 \ u_2 \ u_3 \ u_4]^T \in \mathbb{R}^4$
 186 is the vector of control inputs, S is a torque distribution ma-
 187 trix, $q = [q_{31} \ q_{41} \ q_{32} \ q_{42} \ q_1 \ x \ y]^T \in \mathbb{R}^7$ is the vector of gen-
 188 eralized coordinates (see Fig. 3). Finally, F_{ext} represents the
 189 external forces acting on the robot (contact forces with the
 190 ground). Following the proposed decomposition of the
 191 walking cycle proposed in [12], the walking cycle can be di-
 192 vided into two consecutive phases of motion (see Fig. 4). In
 193 the first one, the biped remains in contact with the ground
 194 through one foot (single support (SS) phase). The other
 195 one is the impact phase [3] that is often considered as instan-
 196 taneous and characterized by a collision between the swing
 197 leg and the ground. Since the assumption that the robot is
 198 walking on horizontal surface without obstacles is made,
 199 the switching from one walking phase to another is closely
 200 related to the vertical position of the robot free leg tip. Let
 201 this position be denoted by $\sigma(q)$, the stance leg is denoted by
 202 (q_{31}, q_{41}) , and the swing leg by (q_{32}, q_{42}) , therefore



Fig. 1. RABBIT prototype testbed.



Fig. 2. The guidance device.

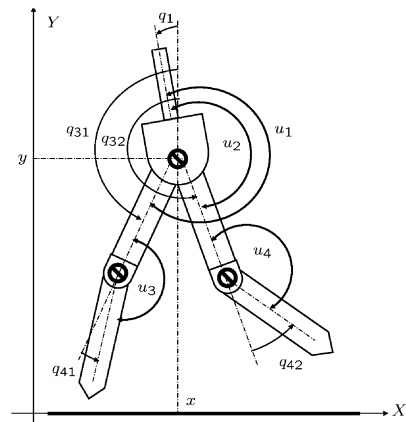


Fig. 3. Schematic view of RABBIT's mechanical structure.

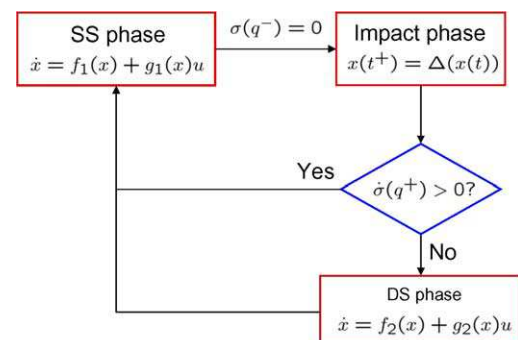


Fig. 4. The walking cycle decomposition.

¹ For a detailed information, see <http://robot-rabbit.lag.ensieg.inpg.fr/>.

$$\sigma(q) = l_3(\cos(q_{32}) - \cos(q_{31})) + l_4(\cos(q_{32} + q_{42}) - \cos(q_{31} + q_{41})) \quad (2)$$

Indeed the impact between the swing leg and the ground² occurs when the foot hits the ground, which can be expressed as

$$\sigma(q) = 0; \quad \dot{\sigma}(q) < 0$$

and it characterizes the switch from the single support phase to the impact phase (cf. Fig. 4). On the other hand, the lift-off from ground occurs just after the impact [3] and may be expressed as (after re-labelling the variables)

$$\sigma(q^+) = 0; \quad \dot{\sigma}(q^+) > 0$$

and it characterizes the switch from the impact phase to the single support phase (cf. Fig. 4). Note that q^+ denotes the vector of the generalized coordinates just after the impact (cf. Section 2.1.2). In the following sections, the dynamic equations for these two phases are presented.

2.1.1. The single support phase model

In this phase only one foot is grounded, and the biped is modelled by the following differential equation [32]:

$$M(q)\ddot{q} + N(q, \dot{q})\dot{q} + G(q) = Su + J_1^T(q)\lambda \quad (3)$$

where $J_1(q)$ represents the Jacobian matrix of the holonomic contact constraints, and λ the Lagrange multipliers of contact forces. Assuming that (q_{31}, q_{41}) is the stance leg, the contact constraints may be expressed by

$$y_{p_1} = \dot{y}_{p_1} = \ddot{y}_{p_1} = 0; \quad x_{p_1} = \dot{x}_{p_1} = \ddot{x}_{p_1} = 0 \quad (4)$$

where (x_{p_1}, y_{p_1}) denotes the cartesian coordinates of the stance leg's foot, given by

$$\begin{cases} y_{p_1}(q) = y + l_3 \cos(q_{31}) + l_4 \cos(q_{31} + q_{41}) \\ x_{p_1}(q) = x - l_3 \sin(q_{31}) - l_4 \sin(q_{31} + q_{41}) \end{cases} \quad (5)$$

Using (5) and (4) one obtains

$$J_1(q)\ddot{q} + \Pi_2(q, \dot{q}) = 0 \quad (6)$$

where $\Pi_2(q, \dot{q})$ is defined by

$$\Pi_2(q, \dot{q}) := \begin{pmatrix} -l_3\dot{q}_{31}^2 \cos(q_{31}) - l_4(\dot{q}_{31} + \dot{q}_{41})^2 \cos(q_{31} + q_{41}) \\ l_3\dot{q}_{31}^2 \sin(q_{31}) + l_4(\dot{q}_{31} + \dot{q}_{41})^2 \sin(q_{31} + q_{41}) \end{pmatrix}$$

The constrained dynamic model in the single support phase is then given by

$$\begin{cases} M(q)\ddot{q} + N(q, \dot{q})\dot{q} + G(q) = Su + J_1^T(q)\lambda \\ J_1(q)\ddot{q} + \Pi_2(q, \dot{q}) = 0 \end{cases} \quad (7)$$

In simulation of the walking robot during the single support phase, a reduced order dynamic model, computed form (7), is used (cf. [7] and the references inside for more details).

2.1.2. The impact phase model

According to [15], the impact between the swing leg and the ground is considered as a rigid collision [3], it occurs when the swing leg hits the walking surface and it induces discontinuities (jumps) in the generalized velocities,³ our objective is then to derive the post-impact velocities in terms of pre-impact positions and velocities. During the impact we have

$$M(q)\ddot{q} + N(q, \dot{q})\dot{q} + G(q) = Su + \delta F_{\text{ext}} \quad (8)$$

where F_{ext} represents the external contact forces.

Under suitable assumptions (see e.g. [15]) on the impact phenomenon, one can deduce the external acting forces by integration of (8) over the impact duration, so one obtains

$$M(q)(\dot{q}^+ - \dot{q}^-) = F_{\text{ext}} = J_2^T(q)\lambda \quad (9)$$

where \dot{q}^+ (respectively, \dot{q}^-) is the velocity just after (respectively before) impact, and $F_{\text{ext}} = \int_{t^-}^{t^+} \delta F_{\text{ext}}$. $J_2(q)$ is the Jacobian matrix of the cartesian coordinates of the swing leg foot, given by

$$\begin{cases} y_{p_2}(q) = y + l_3 \cos(q_{32}) + l_4 \cos(q_{32} + q_{42}) \\ x_{p_2}(q) = x - l_3 \sin(q_{32}) - l_4 \sin(q_{32} + q_{42}) \end{cases} \quad (10)$$

Eq. (9) involves seven constraints and nine unknowns F_{ext} and \dot{q}^+ . Two additional equations may be obtained from the condition that the impacted leg does not rebound nor slips at impact, that is

$$y_{p_2} = \dot{y}_{p_2} = 0; \quad x_{p_2} = \dot{x}_{p_2} = 0 \quad (11)$$

which gives using the expressions of x_{p_2}, y_{p_2}

$$J_2(q)\dot{q}^+ = 0 \quad (12)$$

The solution of (9)–(12) leads to

$$\begin{cases} \dot{q}^+ = \left[I - M^{-1}J_2^T(J_2M^{-1}J_2^T)^{-1}J_2 \right] \dot{q}^- = D(q)\dot{q}^- \\ \lambda = -\left[(J_2M^{-1}J_2^T)^{-1}J_2 \right] \dot{q}^- \end{cases} \quad (13)$$

On the other hand, the impact model must account for the re-labelling of the robot coordinates (i.e. the swing leg becomes the new stance leg and vice versa), this can be expressed by

$$\begin{pmatrix} q^+ \\ \dot{q}^+ \end{pmatrix} = R(q) \begin{pmatrix} q^- \\ \dot{q}^- \end{pmatrix} \quad (14)$$

To summarize, the global impact model that includes both the jumps in velocities and the permutation of coordinates and velocities shortly writes

$$\begin{pmatrix} q^+ \\ \dot{q}^+ \end{pmatrix} = \Delta(q) \begin{pmatrix} q^- \\ \dot{q}^- \end{pmatrix} \quad (14)$$

² The system looks like a kinematic chain [15].

³ But the generalized positions still unaltered i.e. $q^+ = q^- = q$.

304 where

$$\Delta(q) = \begin{pmatrix} R(q) & 0 \\ 0 & R(q)D(q) \end{pmatrix} R = \begin{pmatrix} 0 & 0 & 1 & 0 & 0 & 0 & 0 \\ 0 & 0 & 0 & 1 & 0 & 0 & 0 \\ 1 & 0 & 0 & 0 & 0 & 0 & 0 \\ 0 & 1 & 0 & 0 & 0 & 0 & 0 \\ 0 & 0 & 0 & 0 & 1 & 0 & 0 \\ 0 & 0 & 0 & 0 & 0 & 1 & 0 \\ 0 & 0 & 0 & 0 & 0 & 0 & 1 \end{pmatrix}$$

306

307 3. The key idea: a predictive control scheme

308 Under single support assumption, the five independent
309 degrees of freedom can be subdivided into two parts

$$311 z_1 := q_1 \in \mathbb{R}; \quad z_2 := (q_{31} \quad q_{41} \quad q_{32} \quad q_{42})^T \in \mathbb{R}^4$$

312 where z_2 can be assumed to be completely controllable
313 (provided that saturation constraints on actuators and con-
314 tact conditions are fulfilled). In this section, the sequence of
315 impact instants is denoted by $(t_k)_{k \in \mathbb{N}}$ with $t_k = kt_f$ where t_f
316 is the step duration.

317 **Remark 1.** Under nominal conditions, the step duration t_f
318 is fixed and it does not change from one step to another,
319 nevertheless if the biped is required to change the walking
320 speed, among others, a solution could be investigated to
321 change this parameter, but for each speed and configura-
322 tion corresponds a well specified value of t_f .

323 Let us choose some target configuration $z_2^f \in \mathbb{R}^4$ (cf. Sec-
324 tion 5.1) that is to be reached just before the impact
325 instants t_k that is $z_2(t_k^-) = z_2^f$. This choice is fixed in all
326 the forthcoming developments, in a way, z_2^f has to be con-
327 sidered as a design parameter. The way z_2^f may be parame-
328 terized is explained in Section 5.1.

329 Associated to this choice of z_2^f , the following choice
330 $\dot{z}_2^f(z_2^f) \in \mathbb{R}^4$ is done for the desired $\dot{z}_2(t_k^-)$, this choice is
331 defined given some desired foot impact velocity $-v_{p_2}$
332

$$334 \begin{aligned} \dot{z}_2^f(z_2^f, v_{p_2}) &:= \text{Arg min}_{\dot{z}_2} \|\dot{z}_2\|^2 \quad \text{under} \quad \frac{\partial y_{p_2}}{\partial z_2}(z_2^f) \dot{z}_2 = -v_{p_2} \\ &= - \left[\frac{\partial y_{p_2}}{\partial z_2}(z_2^f) \right]^T v_{p_2} / \left\| \frac{\partial y_{p_2}}{\partial z_2}(z_2^f) \right\|^2 \end{aligned} \quad (15)$$

335 where $y_{p_2}(z_2)$ is the y -coordinate of the swing foot. There-
336 fore, \dot{z}_2^f is clearly the minimum norm velocity vector that
337 corresponds to some impact velocity $-v_{p_2}$. Once this choice
338 is done, a final desired “just before impact” sub-state
339 $(z_2, \dot{z}_2) \in \mathbb{R}^8$ is completely defined by the choice of $z_2^f \in \mathbb{R}^4$.

340 In what follows, the following notations are used
341

$$343 \begin{aligned} \mathcal{Z}_2 &:= \begin{pmatrix} z_2 \\ \dot{z}_2 \end{pmatrix} \in \mathbb{R}^8; \quad \mathcal{Z}_2^f := \begin{pmatrix} z_2^f \\ \dot{z}_2^f(z_2^f, v_{p_2}) \end{pmatrix} \in \mathbb{R}^8; \\ \mathcal{Z}_1 &:= \begin{pmatrix} q_1 \\ \dot{q}_1 \end{pmatrix} \in \mathbb{R}^2 \end{aligned} \quad (16)$$

Now, during the step, let us denote by $\eta > 0$ the remaining
time before impact. One has the following dynamic for η

$$\dot{\eta} = -1 + \delta(\eta) \cdot t_f \quad (17)$$

where $\delta(\cdot)$ is the generalized impulse function. Consider a
control sampling period $\tau_c > 0$ such that $t_f/\tau_c = N_c \in \mathbb{N}$
(N_c : is also a design parameter).

Basically, a problem of synchronizing the sampling
times to the impact times could appear when impact is
either detected prematurely (i.e. before the expected
instant) or detected with a delay (i.e. after the expected
instant). Since RABBIT PROTOTYPE feet are equipped with
switches, the impact instant could easily be detected. This
situation is managed as indicated in Section 4.3 concerning
implementation issues.

Let us use the following notation to refer to decision
instants [4] on the interval $[t_k, t_{k+1}]$

$$\tau_k^i = t_k + i\tau_c; \quad i \in \{0, \dots, N_c - 1\}; \quad k \in \mathbb{N}$$

During the step, at each decision instant τ_k^i , a p -parameter-
ized reference trajectory⁴

$$\mathcal{Z}_2^{\text{ref}}(\tau', \mathcal{Z}_2(\tau_k^i), \mathcal{Z}_2^f, \eta(\tau_k^i), p); \quad \tau' \in [\tau_k^i, t_{k+1}]; \quad p \in \mathcal{P} \quad (18)$$

is defined that satisfies for all parameter value $p \in \mathcal{P}$ the
following boundary (initial and final) conditions

$$\mathcal{Z}_2^{\text{ref}}(\tau_k^i, \mathcal{Z}_2(\tau_k^i), \mathcal{Z}_2^f, \eta(\tau_k^i), p) = \mathcal{Z}_2(\tau_k^i) \quad (19)$$

$$\mathcal{Z}_2^{\text{ref}}(t_{k+1}, \mathcal{Z}_2(\tau_k^i), \mathcal{Z}_2^f, \eta(\tau_k^i), p) = \mathcal{Z}_2^f \quad (20)$$

namely, the reference trajectory $\mathcal{Z}_2^{\text{ref}}(\cdot, \mathcal{Z}_2(\tau_k^i), \mathcal{Z}_2^f, \eta(\tau_k^i), p)$
is updated at each decision instant τ_k^i to start at the present
value $\mathcal{Z}_2(\tau_k^i)$, and to join the desired final value \mathcal{Z}_2^f just be-
fore next impact.

It is worth noting that $p \in \mathcal{P}$ is the remaining free
parameter, once the constraints (19) and (20) have been
structurally imposed, on some initial parameterization.
This is typically easy to realize with polynomial parameter-
ization [9] of trajectories since (19) and (20) are linear con-
straints in the polynomial coefficients.

A relevant question is: how to choose $p \in \mathcal{P}$?

The role of p is clearly to optimize the behavior of the
indirectly controlled sub-state \mathcal{Z}_1 . Indeed, imagine that a
perfect tracking of the reference trajectory $\mathcal{Z}_2^{\text{ref}}(\cdot, \mathcal{Z}_2(\tau_k^i),$
 $\mathcal{Z}_2^f, \eta(\tau_k^i), p)$ is performed over $[\tau_k^i, t_{k+1}]$. What are the con-
sequences of such tracking on the value of both \mathcal{Z}_1 and \mathcal{Z}_2
just before the $(k+1)$ impact?

- For \mathcal{Z}_2 , one would clearly have, because of the perfect tracking [see (20)]

$$\mathcal{Z}_2(t_{k+1}^-) = \mathcal{Z}_2^f \quad (21)$$

- For the \mathcal{Z}_1 dynamic, let us consider the torso equation extracted from the dynamic model (1), and given by

⁴ In [16] for instance such trajectories are generated using Van der Pol oscillators.

$$\left(\frac{1}{4}m_1 l_1^2 + I_1\right)\ddot{q}_1 = \frac{1}{2}m_1 l_1 \cos(q_1)\ddot{x} + \frac{1}{2}m_1 l_1 \sin(q_1)(\ddot{y} + g) - u_1 - u_2 \quad (22)$$

where m_1 is the mass of the torso, l_1 its length, u_1 and u_2 are the torques of the femurs.

Using Eqs. (4) and (5) and notations (16), this dynamic should be written

$$\dot{\mathcal{Z}}_1 = f(\mathcal{Z}_1, \mathcal{Z}_2, u) \quad (23)$$

The closed-loop system is obtained by state feedback, that is $u = K(\mathcal{Z}, \mathcal{Z}_2^{\text{ref}})$, therefore equation (23) could be rewritten as

$$\dot{\mathcal{Z}}_1 = f(\mathcal{Z}_1, \mathcal{Z}_2, \mathcal{Z}_2^{\text{ref}}) \quad (24)$$

Under the assumption of perfect tracking, by replacing \mathcal{Z}_2 in (24) by the reference trajectory $\mathcal{Z}_2^{\text{ref}}$ ⁵ one obtains:

$$\dot{\mathcal{Z}}_1 = f(\mathcal{Z}_1, \mathcal{Z}_2^{\text{ref}}) = f(\mathcal{Z}_1, \mathcal{Z}_2(\tau_k^i), \mathcal{Z}_2^f, p) \quad (25)$$

and integrating (25) starting from the initial condition $(\tau_k^i, \mathcal{Z}_1(\tau_k^i))$ gives the predicted value of $\mathcal{Z}_1(t_{k+1}^-)$ just before next impact. This can be rewritten formally as follows $(\eta(\tau_k^i) = t_{k+1} - \tau_k^i)$

$$\widehat{\mathcal{Z}}_1(t_{k+1}^- | \tau_k^i) = \Psi(\mathcal{Z}_1(\tau_k^i), \mathcal{Z}_2(\tau_k^i), \mathcal{Z}_2^f, \eta(\tau_k^i), p) \quad (26)$$

and using the impact equation (cf. Eq. (14)) together with the predicted values (21) and (26) one can derive an expression of the predicted value of \mathcal{Z}_1 just after impact

$$\widehat{\mathcal{Z}}_1(t_{k+1}^+ | \tau_k^i) = \Psi^+(\mathcal{Z}_1(\tau_k^i), \mathcal{Z}_2(\tau_k^i), \mathcal{Z}_2^f, \eta(\tau_k^i), p) \quad (27)$$

The value of the reference trajectory's parameter $p(\tau_k^i)$ is then given by the optimal solution of the following quadratic optimization problem

$$\hat{p}(\tau_k^i) = \min_{p \in \mathcal{P}} \|\widehat{\mathcal{Z}}_1(t_{k+1}^+ | \tau_k^i) - \mathcal{Z}_1^f\|_Q^2 \text{ subject to} \\ C(\mathcal{Z}_2(\tau_k^i), \mathcal{Z}_2^f, p) > 0; \quad Q \in \mathbb{R}^{2 \times 2} \quad Q > 0 \quad (28)$$

where

- $\mathcal{Z}_1^f \in \mathbb{R}^2$ is some desired value just after the impact. This value (together with \mathcal{Z}_2^f) defines the limit cycle one aims to establish.
- $C(\mathcal{Z}_2(\tau_k^i), \mathcal{Z}_2^f, p) > 0$ is a constraint expressing non penetration condition. This can be for instance

$$C(\mathcal{Z}_2(\tau_k^i), \mathcal{Z}_2^f, p) := \min_{\tau' \in [\tau_k^i, \tau_{k+1}^i - \epsilon]} y_{p_2}(\tau', \mathcal{Z}_2(\tau_k^i), \mathcal{Z}_2^f, p) \quad (29)$$

for some small $\epsilon > 0$.

To summarize,⁶ during the step, at each decision instant τ_k^i with $i < N_c - 1$ the reference trajectory

$$\mathcal{Z}_2^{\text{ref}}(\tau', \mathcal{Z}_2(\tau_k^i), \mathcal{Z}_2^f, \eta(\tau_k^i), \hat{p}(\tau_k^i)); \quad \tau' \in [\tau_k^i, t_{k+1}] \quad 449$$

is defined on the completely controlled variables (actuated joints) and tracked using a nonlinear time varying feedback during the time interval $[\tau_k^i, \tau_{k+1}^i]$. At the next decision instant τ_{k+1}^i a new reference trajectory

$$\mathcal{Z}_2^{\text{ref}}(\tau', \mathcal{Z}_2(\tau_{k+1}^i), \mathcal{Z}_2^f, \eta(\tau_{k+1}^i), \hat{p}(\tau_{k+1}^i)); \quad \tau' \in [\tau_k^i, t_{k+1}] \quad 455$$

is defined, based on the new measurements and is tracked during the time interval $[\tau_{k+1}^i, \tau_{k+2}^i]$ and the scheme is repeated until the impact instant. This defines a predictive control scheme in which the open-loop auxiliary optimization problem is given by (28). The solution of such optimization problem is performed using the DBCPOL function from the IMSL math library of Digital Fortran 5.0.

4. Stability and implementation issues

The stability can be investigated using the Poincaré's section [17] just before the impact, namely at instants t_k^- . Indeed, if this discrete-time map converges, then a cyclic trajectory results (see Figs. 5 and 6). To study the stability of the Poincaré's map, note that, by definition of the predictive control strategy depicted in the previous section, one clearly has

$$\mathcal{Z}_2(t_k^-) = \mathcal{Z}_2^f \quad (30)$$

where \mathcal{Z}_2^f is the desired final "just before impact" configuration defined by (15) and (16) and depending only on the desired final position z_2^f . Consequently, the overall stability depends on the stability of the sequence

$$(\mathcal{Z}_1(t_k^-))_{k \in \mathbb{N}} \quad 479$$

under the constraint (30).

4.1. Stability definition

As it can be easily understood from Figs. 5 and 6, an asymptotically stable k_0 -cyclic trajectory on the whole state results whenever the following property holds for the closed-loop system's behavior:

$$\|\mathcal{Z}_1(t_{(j+1)k_0}^-) - \mathcal{Z}_1^f\|_Q^2 \leq \mu \|\mathcal{Z}_1(t_{jk_0}^-) - \mathcal{Z}_1^f\|_Q^2; \quad \mu < 1 \quad (31)$$

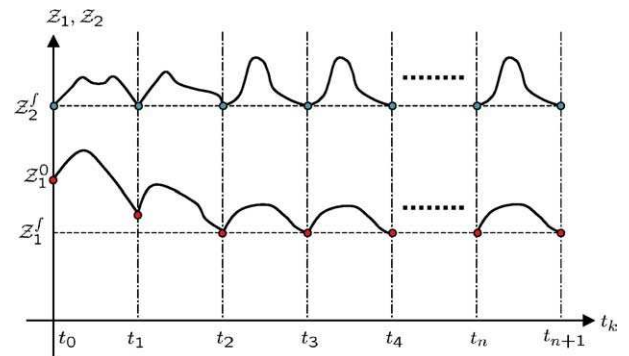


Fig. 5. Stability illustration ($k_0 = 1$).

⁵ Recall that $\mathcal{Z}_2^{\text{ref}}$ depends on $\mathcal{Z}_2(\tau_k^i)$, \mathcal{Z}_2^f , and p .

⁶ A chart flow better illustrating the principle of the approach is given in Section 4.3.

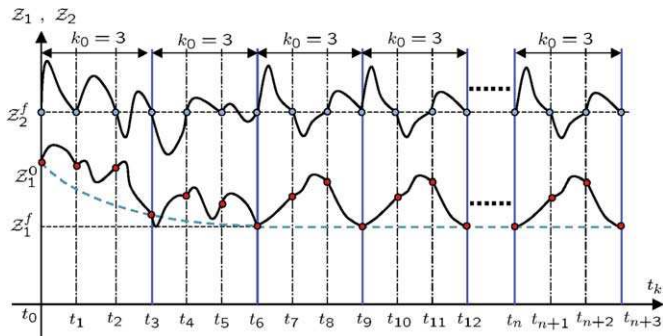


Fig. 6. Stability illustration ($k_0 = 3$).

488 similarly, a neighborhood of a k_0 cyclic trajectory on the
 489 whole is asymptotically stabilized whenever the following
 490 property holds for some small $\varepsilon > 0$,

492
$$\lim_{j \rightarrow \infty} \|\mathcal{Z}_1(t_{jk_0}^-) - \mathcal{Z}_1^f\|_Q^2 \leq \varepsilon \quad (32)$$

493 The aim of the following section is to give sufficient condi-
 494 tions under which one of the above conditions is satisfied
 495 for some $k_0 \in \mathbb{N}$ with a graphical tools enabling a concrete
 496 evaluation of the associated conditions (see Proposition 1
 497 hereafter).

498 4.2. Stability result

499 Now let $\mathcal{Z}_1(t_k^-)$ be given. Using (30) and the impact map
 500 (14), the value of the whole $\mathcal{Z}(t_k^+)$ just after the impact can
 501 be computed and the predictive control closed-loop trajec-
 502 tories may be predicted over $[t_k^+, t_{k+1}^-]$. Therefore, the pre-
 503 dicted value of $\mathcal{Z}_1(t_{k+1}^-)$ just before the next impact is
 504 only function of $\mathcal{Z}_1(t_k^-)$, N_c and $\mathcal{Z}^f := (\mathcal{Z}_1^f, \mathcal{Z}_2^f)$, namely

506
$$\mathcal{Z}_1(t_{k+1}^-) =: \Gamma(\mathcal{Z}_1(t_k^-), \mathcal{Z}^f, N_c) \quad (33)$$

507 which is a discrete-time autonomous system (for fixed \mathcal{Z}^f
 508 and N_c) in the sub-state \mathcal{Z}_1 for which stability is to be
 509 investigated. More generally, the following multi-step
 510 map is particularly relevant to assess the stability of the
 511 above predictive control scheme, namely,

514
$$\mathcal{Z}_1(t_{k+k_0}^-) =: \Gamma^{k_0}(\mathcal{Z}_1(t_k^-), \mathcal{Z}^f, N_c) \quad (34)$$

515 where Γ^{k_0} is obtained by repetitive application of $\Gamma(\cdot)$. Note
 516 that this map is easily computable by simulating k_0 steps
 517 under the closed-loop feedback law explained in the previ-
 518 ous section. It is worth noting that such computations are
 519 to be done off-line for stability investigations. The on-line
 520 feedback however is still based on one-step scalar optimiza-
 521 tion as explained in the preceding section. The whole
 522 closed-loop system stability analysis is based on the follow-
 523 ing proposition

524 Proposition 1

525 1. If for some $(k_0, N_c) \in \mathbb{N} \times \mathbb{N}$, there is $q > 0$ such that

$$\sup_{\|\mathcal{Z}_1 - \mathcal{Z}_1^f\|_Q^2 \leq q} \|\Gamma^{k_0}(\mathcal{Z}_1, \mathcal{Z}^f, N_c) - \mathcal{Z}_1^f\|_Q^2 \leq q \quad (35)$$

528 then the predictive control closed-loop leads to a stable
 529 walk for all initial conditions belonging to the set
 530

531
$$\mathcal{C}_0 := \left\{ \mathcal{Z} = \begin{pmatrix} \mathcal{Z}_1 \\ \mathcal{Z}_2^f \end{pmatrix} \text{ s.t. } \mathcal{Z}_1 \in \mathbb{M}_q \right\} \quad (36)$$

534 where for all $q \geq 0$, $\mathbb{M}_q := \left\{ \mathcal{Z}_1 \mid \|\mathcal{Z}_1 - \mathcal{Z}_1^f\|_Q^2 \leq q \right\}$.

535 2. If in addition, the following condition holds for some
 536 $\mu \in [0, 1]$

537 For all $0 < r < q$ $\psi(r, N_c, k_0)$

$$:= \sup_{\|\mathcal{Z}_1 - \mathcal{Z}_1^f\|_Q^2 = r} \|\Gamma^{k_0}(\mathcal{Z}_1, \mathcal{Z}^f, N_c) - \mathcal{Z}_1^f\|_Q^2 \leq \mu \cdot r \quad (37)$$

540 then the closed-loop trajectories asymptotically converges
 541 to a stable limit cycle of length k_0 defined by the pair
 542 $(\mathcal{Z}_1^f, \mathcal{Z}_2^f)$ for all initial conditions in \mathcal{C}_0 .

543 3. If (35) holds, and if (37) holds for all $r \in [\varepsilon, q]$ and
 544 furthermore,

545
$$\sup_{\|\mathcal{Z}_1 - \mathcal{Z}_1^f\|_Q^2 \leq \varepsilon} \|\Gamma^{k_0}(\mathcal{Z}_1, \mathcal{Z}^f, N_c) - \mathcal{Z}_1^f\|_Q^2 \leq \varepsilon; \quad \varepsilon < q \quad (38)$$

548 (see Fig. 7 for a typical situation) then the set

549
$$\mathcal{C}_1 := \left\{ \mathcal{Z} = \begin{pmatrix} \mathcal{Z}_1 \\ \mathcal{Z}_2^f \end{pmatrix} \text{ s.t. } \mathcal{Z}_1 \in \mathbb{M}_\varepsilon \right\} \quad (39)$$

551 is invariant and attractive for all initial conditions in \mathcal{C}_0
 552 (an ε -neighborhood of the limit cycle is reached).
 553
 554

555 Proof

556 1. Straightforward since condition (35) implies that the set
 557 \mathbb{M}_q is invariant under the composed map $\Gamma^{k_0}(\cdot, \mathcal{Z}^f, N_c)$,
 558 more precisely

560
$$\{\mathcal{Z}_1 \in \mathbb{M}_q\} \Rightarrow \{\Gamma^{k_0}(\mathcal{Z}_1, \mathcal{Z}^f, N_c) \in \mathbb{M}_q\} \quad (40)$$

561 Therefore, starting from some initial value $\mathcal{Z}_1^0 \in \mathbb{M}_q$,
 562 the sequence

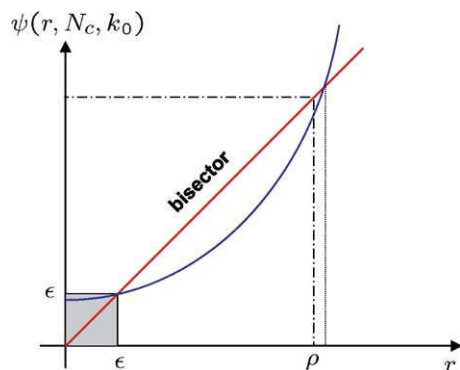


Fig. 7. Typical situation where (35), (37) and (38) hold (point 3 of Proposition 1).

$$564 \quad \left(\mathcal{Z}_1(t_{jk_0}^-) \right)_{j=1}^{\infty}$$

565 belongs to the compact set \mathbb{M}_ϱ .

566 2. Condition (37) implies that for all $j \in \mathbb{N}$, one has

$$569 \quad \|\mathcal{Z}_1(t_{(j+1)k_0}^-) - \mathcal{Z}_1^f\|_Q^2 \leq \mu \|\mathcal{Z}_1(t_{jk_0}^-) - \mathcal{Z}_1^f\|_Q^2 \quad (41)$$

570 (where $\mu < 1$). Accordingly, by recurrence, one obtains
571 (for $m \in \mathbb{N}$)

$$573 \quad \|\mathcal{Z}_1(t_{(j+m)k_0}^-) - \mathcal{Z}_1^f\|_Q^2 \leq \mu^m \|\mathcal{Z}_1(t_{jk_0}^-) - \mathcal{Z}_1^f\|_Q^2 \quad (42)$$

574 which implies that

$$576 \quad \lim_{j \rightarrow \infty} \mathcal{Z}_1(t_{jk_0}^-) = \mathcal{Z}_1^f$$

577 This shows that the closed-loop trajectories tends to a
578 limit cycle of length k_0 defined by the pair of desired val-
579 ues $(\mathcal{Z}_1^f, \mathcal{Z}_2^f)$.

580 3. Using the same argumentation as in the last point, Eq.
581 (41) may be rewritten for all $\mathcal{Z}_1(t_{jk_0}^-)$ that lies in
582 $\mathbb{M}_\varrho \setminus \mathbb{M}_\varepsilon$. This proves that \mathbb{M}_ε is attractive. Further-
583 more, \mathbb{M}_ε is invariant. \square
584

585 Note again that the investigation of (35)–(38) may be
586 done off-line simultaneously and in a deterministic way
587 by solving the following two-dimensional optimization
588 problem

$$590 \quad \psi(r, N_c, k_0) := \sup_{\|\mathcal{Z}_1 - \mathcal{Z}_1^f\|_Q^2 = r} \|I^{k_0}(\mathcal{Z}_1, \mathcal{Z}_1^f, N_c) - \mathcal{Z}_1^f\|_Q^2$$

591 for increasing values of r and check whether the curve so ob-
592 tained [see Fig. 7] satisfies (35)–(38) for some $\varrho > 0$ and
593 $\varepsilon > 0$. The whole procedure may be repeated for different
594 values of k_0 . Concrete examples of such plots are given in
595 Section 5 for a specific choice of the design parameters
596 \mathcal{Z}_1^f , Q and N_c . It is then shown that the condition of point
597 3. of Proposition 1 are satisfied for $k_0 = 3$ (see Fig. 11)
598 while it is not satisfied for $k_0 = 1, 2$. This shows the need
599 for non trivial multi-step map (34) in establishing the sta-
600 bility of the underlying closed-loop behaviour.

601 4.3. Implementation issues

602 The reference trajectories (18) are implemented using
603 Matlab cubic spline interpolation functions with various
604 end-conditions. They are parameterized with a free param-
605 eter p which should be computed by solution of the optimi-
606 zation problem (28). The use of the cubic spline functions
607 requires the definition of the end-conditions, in our case
608 they are given by

- 609 • initial-time conditions, given by Eq. (19),
- 610 • intermediate-time conditions, given by the parameter p
611 to be computed,
- 612 • final-time conditions, given by Eq. (20).
613

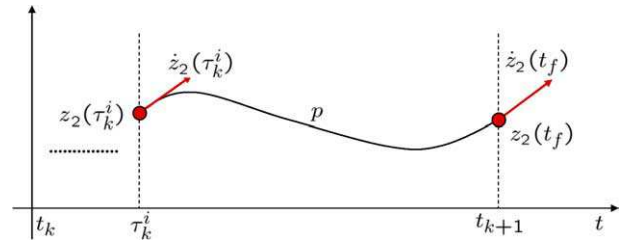


Fig. 8. The directly controlled variables trajectories.

The obtained trajectory, that satisfy these constraints, 614
may be illustrated in Fig. 8. 615

The used subroutines provide the cubic spline interpolant, which should be used to evaluate the trajectory and its derivatives, at each instant τ' . The switching to a new step is closely related to the impact occurrence. The implemented simulator (using visual Fortran 5.0 and Matlab 6.5 softwares) switches to a new step once it detects an impact, therefore three possible cases could be underlined 623

- 624 1. The biped walks without external disturbances, the 624
dynamic model is perfect, as well as the tracking of 625
the optimal reference trajectories. 626
- 627 2. During walking, because of external disturbances, 627
model imperfections, or obstacles, the impact is detected 628
prematurely. 629
- 630 3. The biped, during walking is subject to external distur- 630
bances, model imperfections, or environment changes, 631
as a consequence the impact is not detected at the 632
expected time (instant). 633
634

How the control system would react? 635

In the first case there is no problem, the whole closed-loop system behavior looks like the predicted one. In the second case, when the impact is detected, the reached configuration just after the impact is considered as an initial configuration, the final desired configuration is then computed, and a new step starts (illustrated in simulation 4). While in the third case, the impact is not detected at the expected instant, so the control system proceed to an extrapolation of the computed trajectories (using the Matlab PPVAL function) until the occurrence of the forthcoming impact. The whole control approach is summarized in the diagram depicted in Fig. 9 that illustrates how it works. 648

649 5. Illustrative simulations

650 Consider the biped robot model (7) and (14) with the 650
parameters summarized in Table 1. The control parameter 651
 $N_c = 1$ is used in the following simulations, enabling a large 652
admissible on-line computation time. Indeed, with this 653
choice, $\tau_c = t_f$ and the trajectories being tracked during 654
the step are updated just after each impact. The following 655

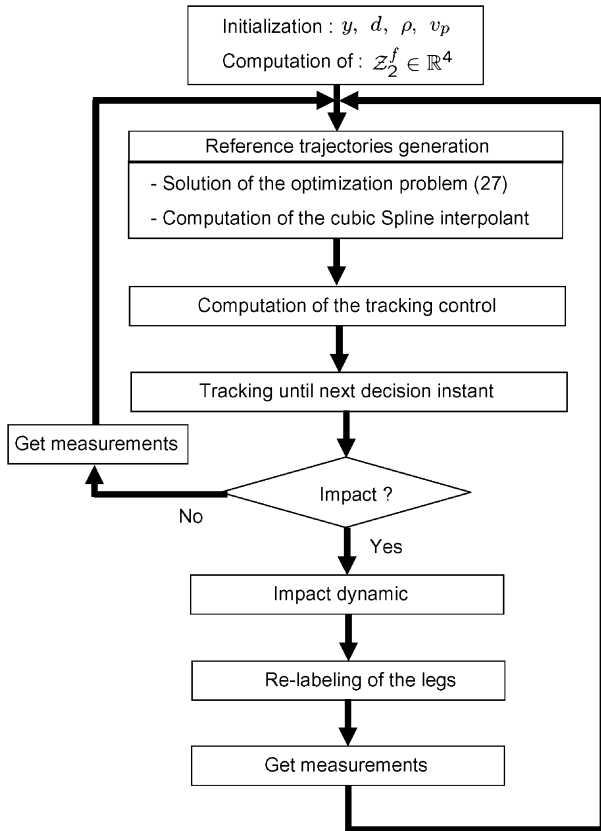


Fig. 9. Algorithm of the approach.

Table 1
The model parameters

Parameter	Mass (kg)	Length (m)	Inertia (kg m ²)
Torso	20	0.625	2.22
Femur	6.8	0.4	1.08
Tibia	3.2	0.4	0.93

- The second one illustrates the transition between several walks with different mean walking velocities.

For robustness evaluation of the proposed controller, two scenarios are investigated, namely

- Robustness against uncertainties in the robot model parameters.
- Robustness against ground irregularities.

Let us first illustrate how z_2^f is chosen by means of a reduced dimensional parameterization. The way such choice of z_2^f may be made optimal in some sense is beyond the scope of the present paper and will be investigated in later works.

5.1. Reduced dimensional parameterization of the position vector z_2

Consider the instantaneous double support configuration. The position vector $z_2 := (q_{31} \ q_{41} \ q_{32} \ q_{42})^T$ is defined by three simple parameters, namely y, d and ρ that are illustrated in Fig. 10.

Indeed, simple computations give

$$\begin{cases} q_{31} = \pi - \arctan\left(\frac{\rho d}{y}\right) - \varphi_{31} \\ q_{32} = \pi + \arctan\left(\frac{(1-\rho)d}{y}\right) - \varphi_{32} \\ q_{41} = \pi - \varphi_{41} = \arccos\left(-\frac{l_3^2 + l_4^2 - \rho^2 d^2 - y^2}{2l_3 l_4}\right) \\ q_{42} = \pi - \varphi_{42} = \arccos\left(-\frac{l_3^2 + l_4^2 - (1-\rho)^2 d^2 - y^2}{2l_3 l_4}\right) \end{cases} \quad (43)$$

where

choice of the parameter p is used in the definition of the predictive control law (see Section 3):

$$p(t_k) := \pi - q_{31}(t_k + t_f/2)$$

Remark 2. The proposed choice of the optimization parameter represents the angular position of the femur of the swing leg at median instant between two impacts. This is a particular choice among many others, for instance one can imagine any free parameter on the trajectories of the actuated coordinates or their derivatives, it can also be one of the configuration parameters (ρ for instance).

Two simulation scenarios are proposed:

- The first one shows how the biped reaches a stable walk with constant mean velocity starting from rest.

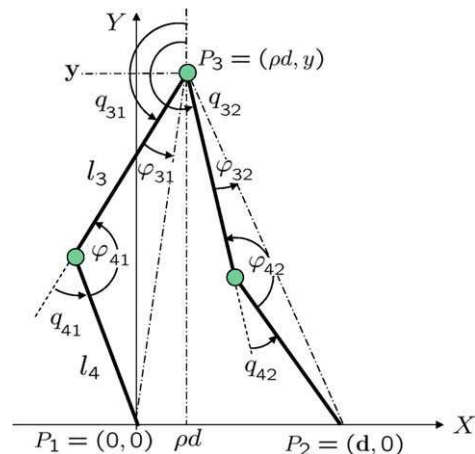


Fig. 10. Computation scheme for the position's reduced parameterization.

$$\left\{ \begin{array}{l} \varphi_{31} = \arccos \left(\frac{l_3^2 - l_4^2 + \rho^2 d^2 + y^2}{2l_3 \sqrt{\rho^2 d^2 + y^2}} \right) \\ \varphi_{32} = \arccos \left(\frac{l_3^2 - l_4^2 + (1 - \rho)^2 d^2 + y^2}{2l_3 \sqrt{(1 - \rho)^2 d^2 + y^2}} \right) \\ \varphi_{41} = \arccos \left(\frac{l_3^2 + l_4^2 - \rho^2 d^2 - y^2}{2l_3 l_4} \right) \\ \varphi_{42} = \arccos \left(\frac{l_3^2 + l_4^2 - (1 - \rho)^2 d^2 - y^2}{2l_3 l_4} \right) \end{array} \right. \quad (44)$$

697
698 This enables a simple choice of the desired final configura-
699 tion just before the impact z_2^f using parameters that are di-
700 rectly linked to the mean velocity and the geometric
701 configuration [32].

702 5.2. Simulation 1: cyclic forward walking starting 703 from rest (standing position)

704 The aim of this simulation is to take the robot from a
705 rest position to a constant speed periodic walking. The con-
706 figuration z_2^f and the other control design parameters are
707 summarized in Table 2.

708 5.2.1. Stability analysis according to Proposition 1

709 In this section, it is shown that under the feedback
710 defined above, the sufficient conditions invoked in point
711 3. of Proposition 1 are satisfied. This can be verified on
712 Fig. 11, that shows the multi-step map

$$\psi(r, N_c, k_0) = \sup_{\|\mathcal{Z}_1 - \mathcal{Z}_1^f\|_Q^2 = r} \|I^{k_0}(\mathcal{Z}_1, \mathcal{Z}_1^f, N_c) - \mathcal{Z}_1^f\|_Q^2$$

714
715 invoked in Proposition 1, for the two cases corresponding
716 to $k_0 = 1, 2$. Note that:

- 717 • For $k_0 = 1$ the conditions of Proposition 1 are not satis-
718 fied. Higher values of k_0 must be investigated in order to
719 prove stability of the closed-loop system. Recall that k_0
720 is only an analysis tool and not a design tool.
- 721 • For $k_0 = 2$, the conditions of point 3 of Proposition 1
722 are satisfied with $\varrho \approx 0.56$ and $\varepsilon \approx 0.08$, therefore for
723 all initial conditions in the set \mathcal{C}_0 given by (36) with

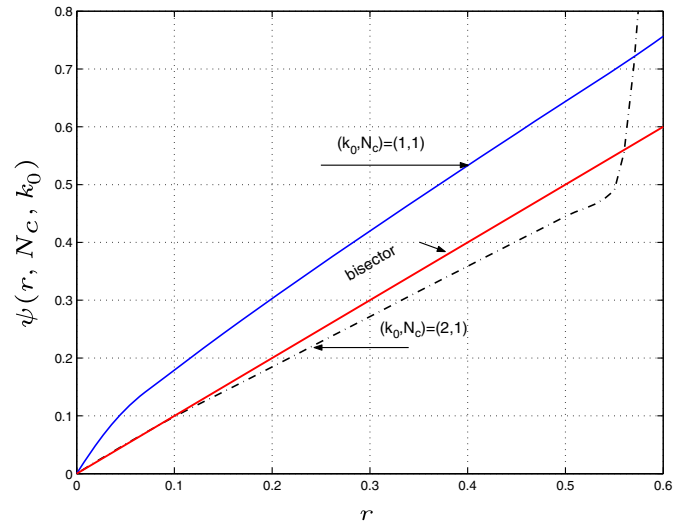


Fig. 11. (Sim 1) A stability analysis tool: the curve $\psi(r, N_c, k_0)$ for different values of k_0 .

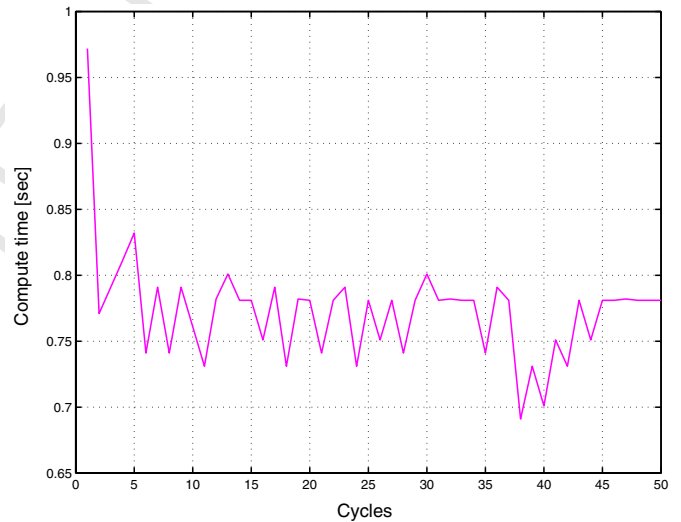


Fig. 12. (Sim 1) Evaluation of computation time.

$$\mathbb{M}_\varrho := \left\{ \mathcal{Z}_1 \mid \|\mathcal{Z}_1 - \mathcal{Z}_1^f\|_Q^2 \leq 0.56 \right\} \quad 725$$

726 the closed-loop trajectories impacts on the Poincaré section
727 converge to the invariant and attractive set \mathcal{C}_1 given
728 by (39) with

$$\mathbb{M}_\varepsilon := \left\{ \mathcal{Z}_1 \mid \|\mathcal{Z}_1 - \mathcal{Z}_1^f\|_Q^2 \leq 0.08 \right\} \quad 730$$

731 which is a neighborhood of the desired limit cycle of
732 length 2 defined by $\mathcal{Z}_1^f = 0$.

733 This example shows clearly the need to the multi-step
734 stability analysis tool developed in Proposition 1, since
735 for $k_0 < 2$, stability cannot be claimed.

736 **Remark 3.** To give some concrete idea about how large is
737 the region of attraction, note that the set of initial
738 conditions \mathbb{M}_ϱ leading to convergence to the neighborhood

Table 2
The approach's parameters description

	Significance	Value
t_f	Step duration	0.75 s
y	Hips height	$y = 0.775$
d	Step length	0.3 m
ρ	Hip's x position w.r.t. step length	0.5
v_p	Foot impact velocity	-0.25 m/s
\mathcal{Z}_{10}	Initial conditions on the torso	(0, 0)
Q	Weighting matrix in optimization	$\begin{pmatrix} 1 & 0 \\ 0 & 0 \end{pmatrix}$
v_{mean}	Mean walking velocity	-0.4 m/s

739 of the limit cycle corresponds, among others to the
 740 following two initial conditions:

742 $(q_1, \dot{q}_1)_0 = (\pm 42.87^\circ, 0^\circ/\text{s})$

743 5.2.2. More simulation results

744 The behavior of the closed-loop system is to be illus-
 745 trated through the following simulation results. In Fig. 13
 746 the phase portrait $(q_1 - \dot{q}_1)$ [16] of the unactuated coordi-
 747 nate (torso) is displayed, where we note the convergence
 748 to a neighborhood of a limit cycle of length 2, which con-
 749 firm the stability result discussed above. The mean walking
 750 velocity evolution is shown in Fig. 14 where the transition
 751 from a rest to the desired mean velocity stable walk can be
 752 observed. Note that the mean velocity is computed as the
 753 ratio between $\Delta x(k)$ and t_f where $\Delta x(k) = x(t_k) - x(t_{k-1})$.
 754 The position and velocity of the torso coordinate is shown
 755 in Fig. 15 where we note through its trajectory that it

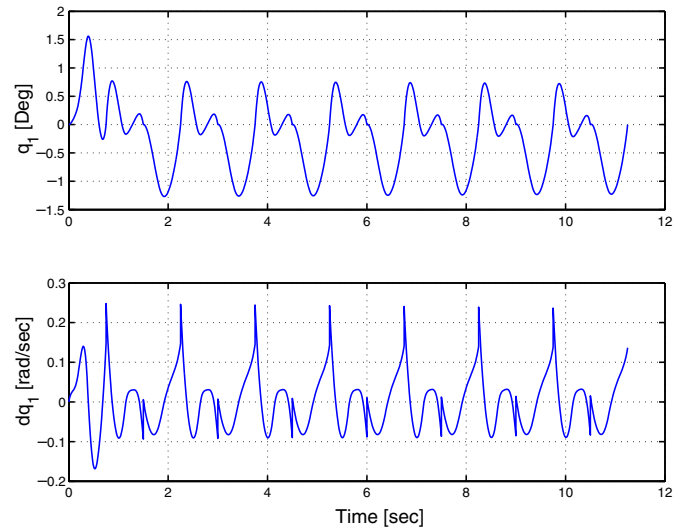


Fig. 15. (Sim 1) The torso position and velocity versus time.

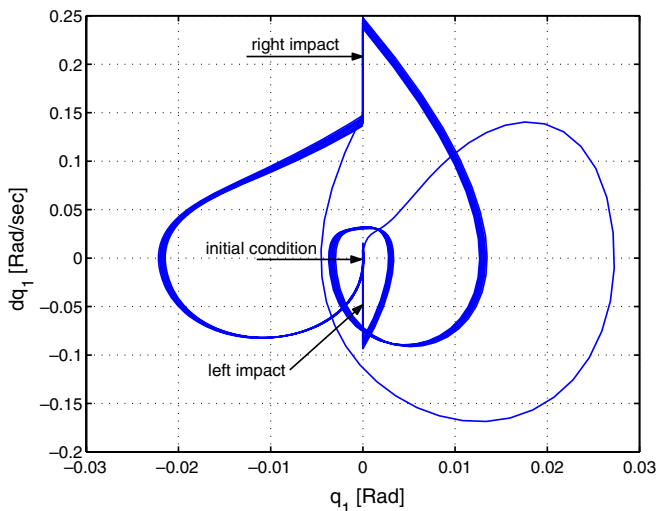


Fig. 13. (Sim 1) The phase portrait of the non actuated coordinate (torso).

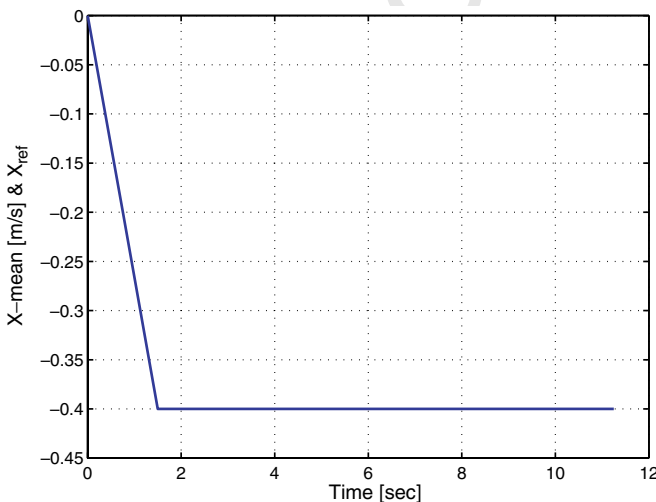


Fig. 14. (Sim 1) The mean walking velocity.

remains close to the vertical. The cartesian coordinates
 (and their corresponding velocities) of the hips are depicted
 in Fig. 17 (for the x coordinate) and in Fig. 18 (for the y
 coordinate), furthermore the resulting trajectory of the hips
 in the plane $x - y$ is illustrated in Fig. 16.

The system control inputs (i.e. joint torques) to be
 applied to the actuated joints are depicted in Fig. 19 for
 both femurs, and in Fig. 20 for both tibias. We note that
 RABBIT is equipped with dc motors of a maximum torque
 of 150 N m, therefore according to the figures of the gener-
 ated torques we conclude that this bound is largely satis-
 fied, but it should also be checked that the power
 requirement remain within the admissible limit.

To check the admissibility of the actuators required
 power, the idea is to plot the angular velocity of the actu-
 ators versus their absolute torques, and check if the
 obtained curves remain within the admissible region given
 by the manufacturer of the actuators (DC motors). If it is

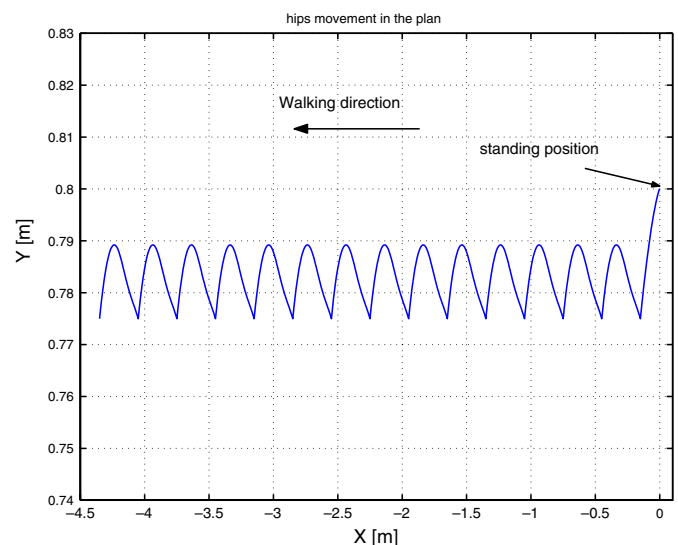


Fig. 16. (Sim 1) The hips movement trajectory.

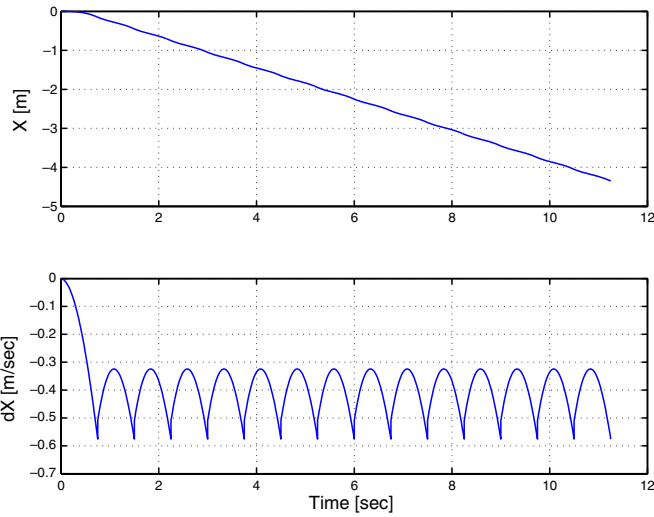


Fig. 17. (Sim 1) The x position and velocity versus time.

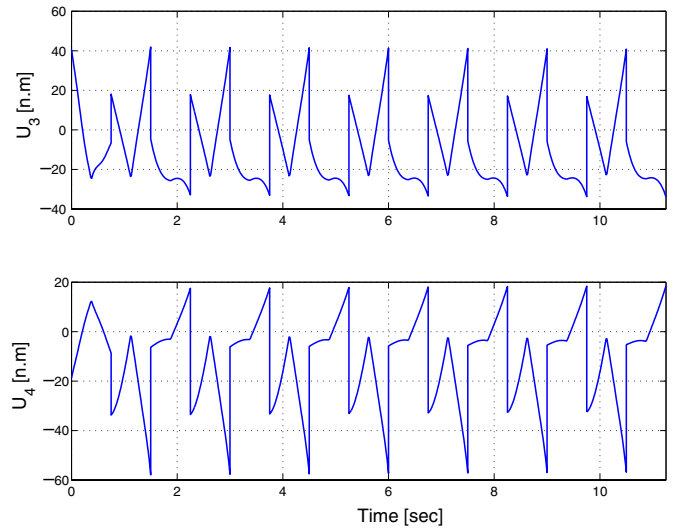


Fig. 20. (Sim 1) The torques of the tibias versus time.

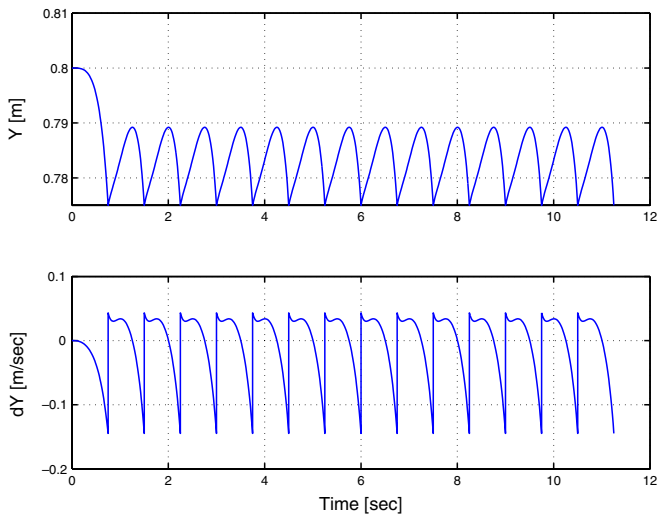


Fig. 18. (Sim 1) The y position and velocity versus time.

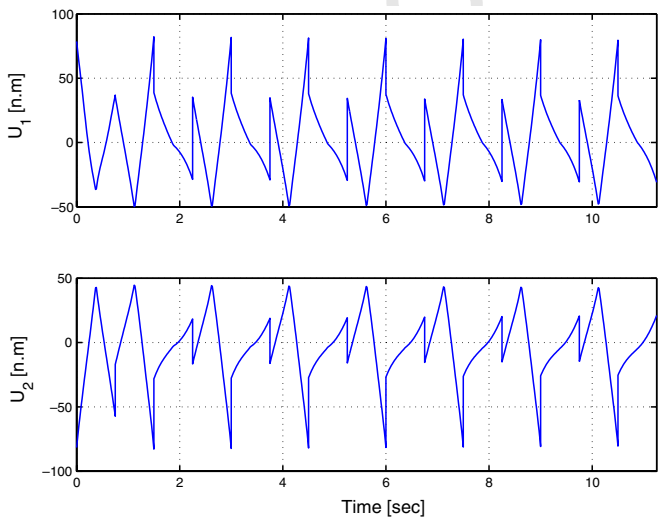


Fig. 19. (Sim 1) The torques of the femurs versus time.

the case it could be concluded that required actuators power is admissible. To compute the velocities of the motors and their absolute torques, based on articular velocities and the motors gear ratio which is of 50, the following formulas are used:

$$\begin{cases} v_{mot} \text{ [rpm]} = \frac{v_{art} \times 50 \times 60}{2 \times \pi} \\ \tau_{mot} \text{ [N m]} = \frac{\tau_{art}}{50} \end{cases} \quad (45)$$

where v_{mot} [rpm] is the velocity of the motor shaft, v_{art} [rad/s] is the relative velocity between the two adjacent links of the concerned articulation, τ_{mot} [N m] is the motor torque, and τ_{art} [N m] is the torque applied on the links.

The application of this verification technique is illustrated on Fig. 21, which depicts the shaft speed versus tor-

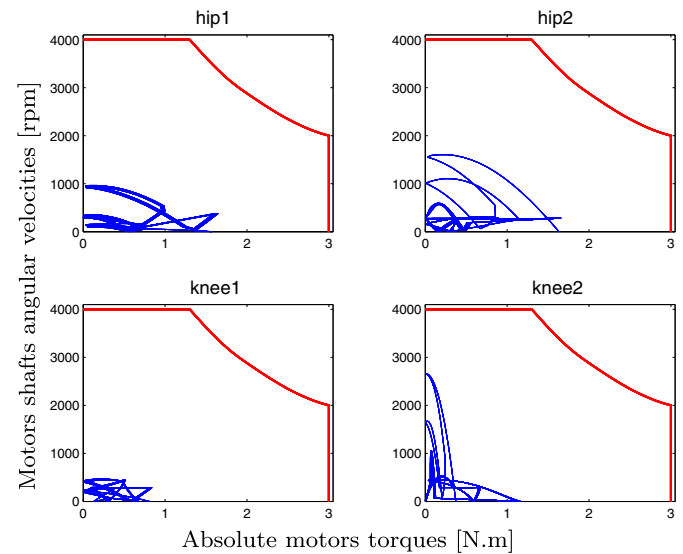


Fig. 21. (Sim 1) Absolute value of actuator angular velocities (revolutions per minute) versus absolute value of actuator torques [N m], and admissible region.

774
775
776
777
778

780

781
782
783
784
785
786

787 que, for the four robot actuators, where it could be clearly
 788 seen that the actuators power requirement is admissible.
 789 The contact foot interaction forces with ground are plotted
 790 versus time in Fig. 22, where we note that the condition of
 791 the friction Coulomb's law is largely satisfied (this is clearly
 792 seen through the amount of the ratio λ_t/λ_n with respect to
 793 the friction coefficient which is $\mu_0 = 0.7$). Fig. 23 illustrates
 794 the movement of the robot by means of a set of walking
 795 stick figures (for the three first steps).

796 5.2.3. Computation time evaluation

797 In order to evaluate the computation time of the pro-
 798 posed control scheme, let us consider biped walking for
 799 50 steps with a constant speed. The evaluation of the com-
 800 puting time is displayed in Fig. 12, which represents the
 801 evolution of the computing time versus cycles (steps). The
 802 maximum value is given by $t_{\max} = 0.97$ s. For real time

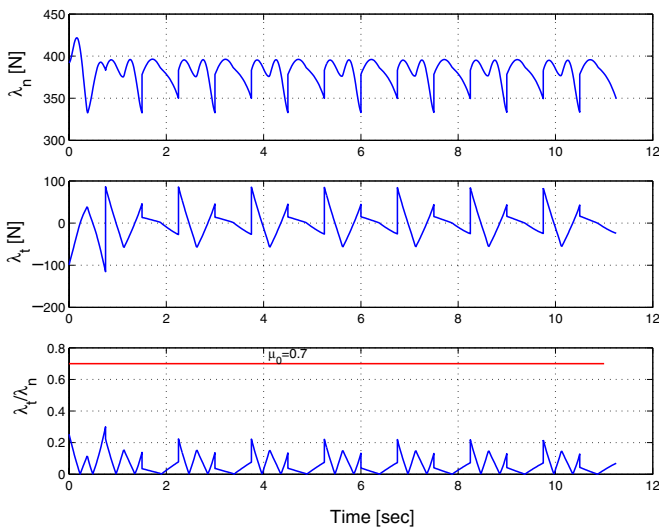


Fig. 22. (Sim 1) The stance foot interaction forces with ground and their ratio (λ_t/λ_n).

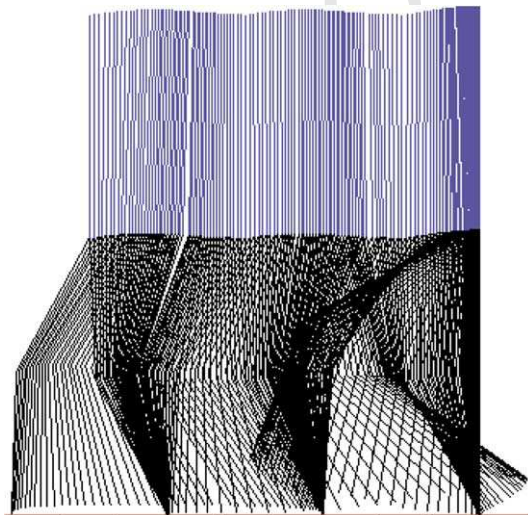


Fig. 23. (Sim 1) Stick figures of the walking robot.

803 implementation the on-line optimization is replaced by an
 804 interpolation procedure. The basic idea is to define a grid
 805 on the space (q_1, \dot{q}_1) , and for all the points the optimization
 806 problem is resolved off-line to define the corresponding
 807 optimization parameter p , so that at the end of the proce-
 808 dure a look-up table is obtained. In the experiments this
 809 look-up table is used to find, for the chosen configuration,
 810 the optimization parameter at each sample time knowing
 811 the initial condition (position and velocity) on the unactu-
 812 ated coordinate.

5.3. Simulation 2: transition between different mean walking velocities

815 In this simulation, it is shown that the proposed feed-
 816 back enables transitions between different mean walking
 817 velocities to be easily obtained. To show this, 46 walking
 818 cycles have been produced during which different desired
 819 velocities of 0.24 m/s, 0.3 m/s and 0.40 m/s are successively
 820 applied during 12, 14 and 20 cycles respectively. Because of
 821 the proportional dependency between the duration of the cycle
 822 t_f and the mean walking speed we have chosen to
 823 change t_f under constant $d = 0.3$ m in order to increase
 824 (go faster), or to decrease (go slower) the walking speed.
 825 Since the step length is 0.3 m, the choice of the cycle end-
 826 time corresponding to the yet mentioned speeds (0.24,
 827 0.3, and 0.40 m/s respectively) is (1.25, 1, and 0.75 s respec-
 828 tively).

829 Fig. 24 shows the phase portrait of the unactuated coordi-
 830 nate (torso), where it is well shown the transition between
 831 the different stable limit cycles (each limit cycle is relative to
 832 a walking speed). In Fig. 25 the mean walking speed is plot-
 833 ted, showing thus the switching between the different pro-
 834 posed walking speeds. The behavior of the unactuated
 835 coordinate (torso) is illustrated in Fig. 26 giving its position
 836 as well as its velocity versus time. The cartesian coordinates
 837 (horizontal, respectively vertical) of the hips are depicted

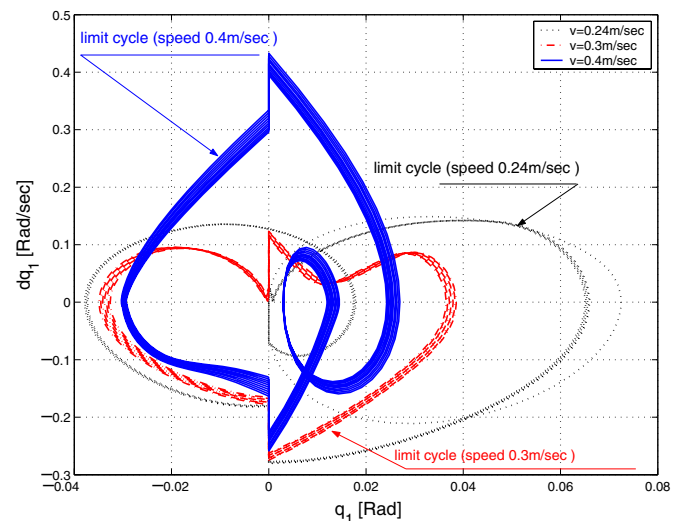


Fig. 24. (Sim 2) The phase portrait of the non actuated coordinate (torso).

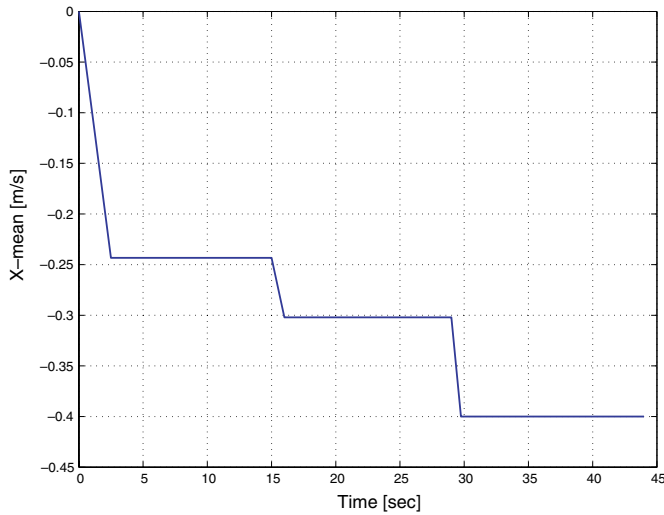


Fig. 25. (Sim 2) The mean walking velocity.

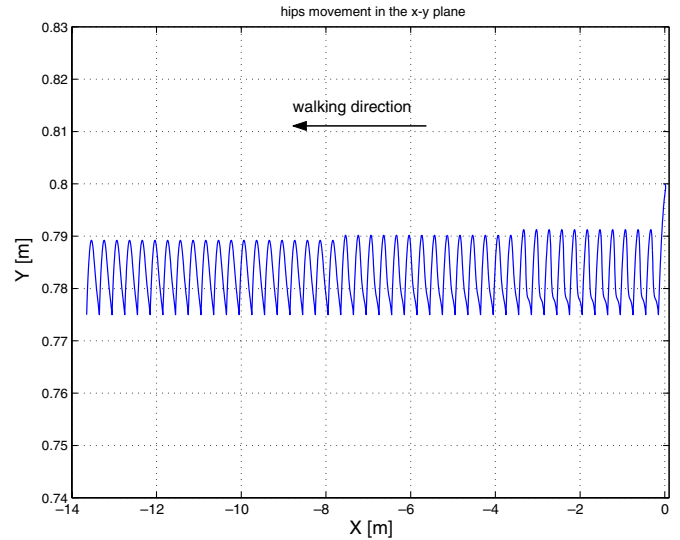


Fig. 27. (Sim 2) The hips movement trajectory.

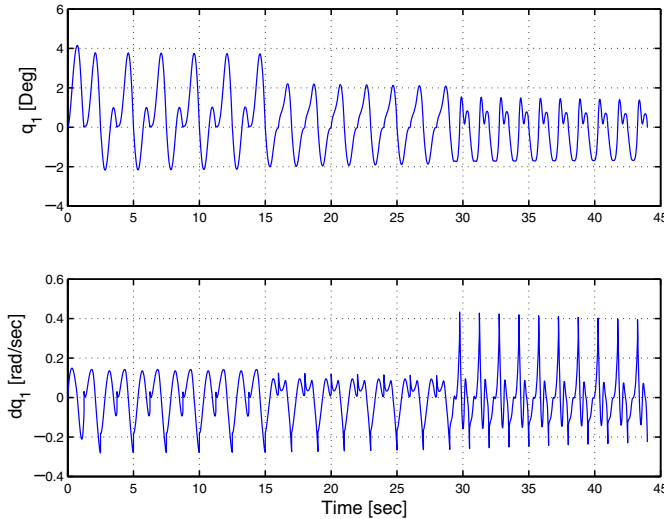


Fig. 26. (Sim 2) The torso position and velocity versus time.

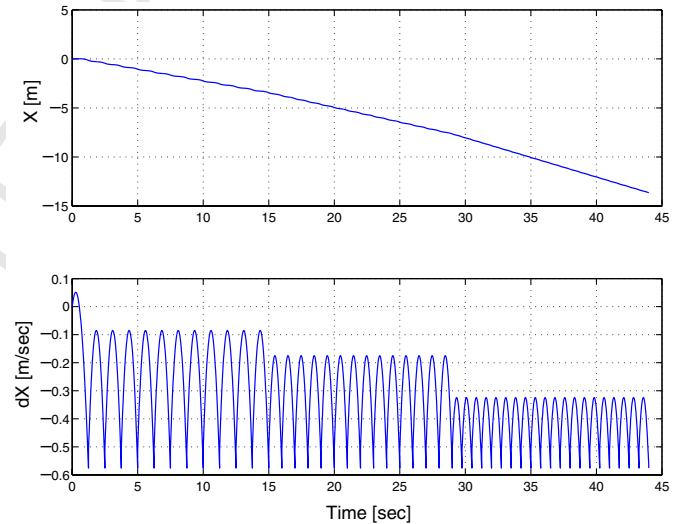


Fig. 28. (Sim 2) The x position and velocity versus time.

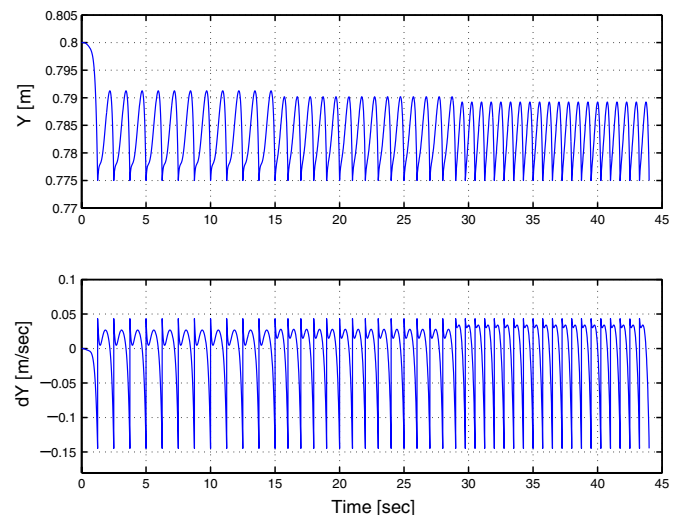


Fig. 29. (Sim 2) The y position and velocity versus time.

838 respectively in Figs. 28 and 29, and a more illustrative plot
839 of the hip's trajectory in the sagittal plane is given in
840 Fig. 27.

841 The generated torques are plotted in Figs. 32 and 33 for
842 the femurs and tibias respectively, while in Fig. 30 it is
843 checked that power requirement remain within the permitted
844 limit. The contact forces with ground of the stance leg
845 foot are depicted in Fig. 31, where we see clearly that the
846 robot keeps contact with ground during walking.

847 5.4. Simulation 3: robustness against parameters 848 uncertainty

849 In order to investigate the robustness of the proposed
850 controller, let us introduce parameter uncertainties. The
851 inertias of the robot links, namely I_1 (the torso), I_3 (the
852 femur) and I_4 (the tibia) cf. Table 1, are considered with
853 an uncertainty of 10% of their nominal values, that is

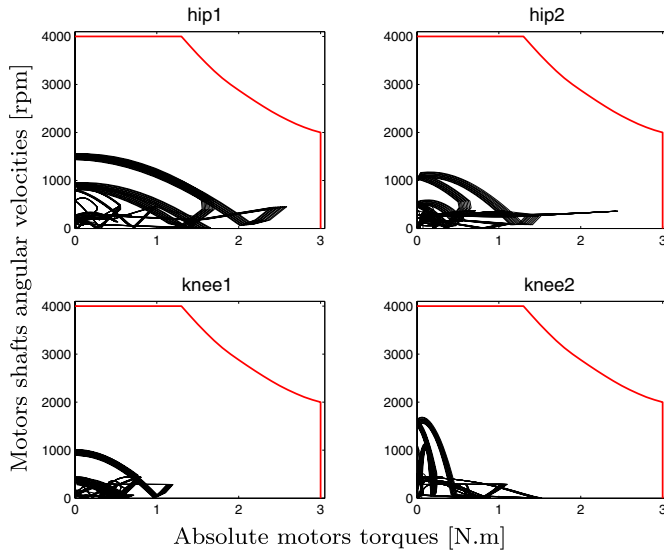


Fig. 30. (Sim 2) Absolute value of actuator angular velocities (revolutions per minute) versus absolute value of actuator torques [N.m], and admissible region.

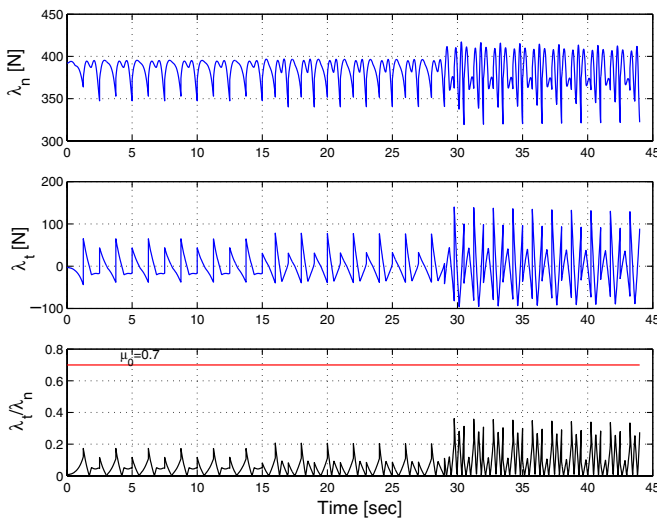


Fig. 31. (Sim 2) The stance foot interaction forces with ground and their ratio λ_t/λ_n .

$$855 \quad I_{1u} = I_1 + \Delta I_1; \quad I_{3u} = I_3 + \Delta I_3; \quad I_{4u} = I_4 + \Delta I_4$$

856 where the uncertainties $\Delta I_i = 0.1I_i$, for $i \in \{1, 3, 4\}$. Figs.
857 34–39 present the corresponding simulation results over
858 12 walking steps.

859 In Fig. 34 the positions and velocities of the first leg
860 femur are plotted for the nominal system (solid line), as
861 well as for the uncertain system (dashed line). Whereas in
862 Fig. 35, the positions and velocities of the tibia are plotted.
863 It can be seen clearly that the introduced uncertainty affects
864 more the femur coordinates.

865 The behavior of the unactuated coordinate (torso) is
866 represented in Fig. 36 which plots the evolution of its posi-
867 tion and velocity versus time. A convergence to a new stable
868 cyclic trajectory is observed. This fact can be seen also

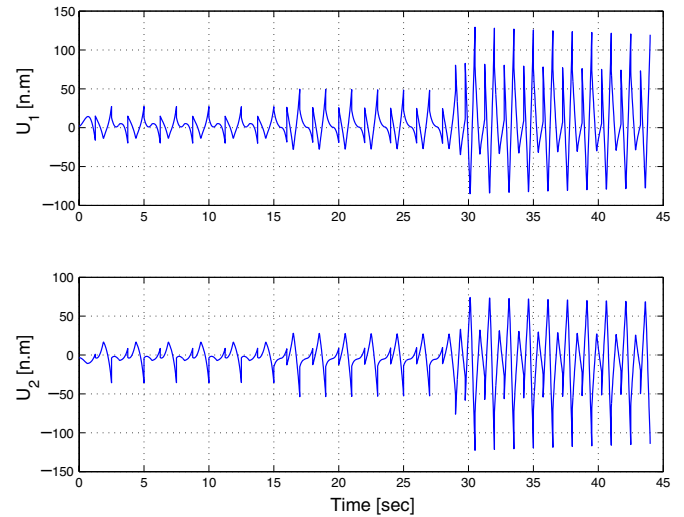


Fig. 32. (Sim 2) The torques of the femurs versus time.

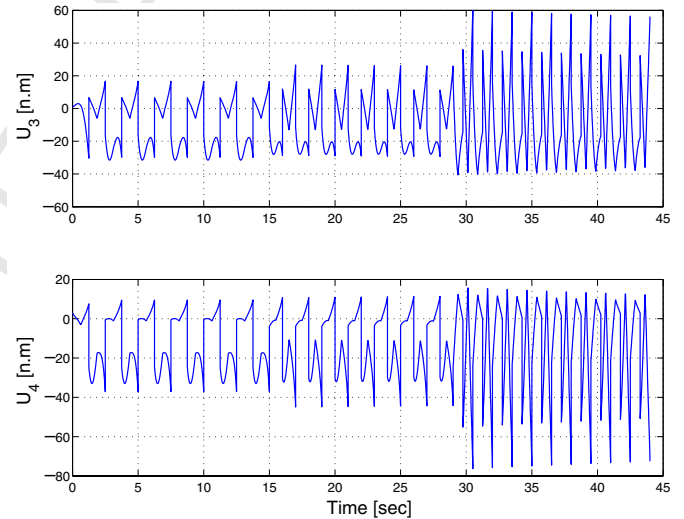


Fig. 33. (Sim 2) The torques of the tibias versus time.

869 on the phase portrait of Fig. 37, where a convergence to a
870 neighborhood of a new limit cycle (different from that of
871 the nominal system) of length 2 is observed for the uncertain
872 system.

873 In Figs. 38 and 39 the control inputs of the robot are
874 plotted, they represent the torques generated by the pro-
875 posed controller for the femurs articulations (Fig. 38) and
876 for the tibias articulations (Fig. 39). For both figures the
877 uncertain system torques are slightly different from those
878 of the nominal system.

879 Let us now consider an other test of the robustness of
880 the proposed control approach. This time consider an
881 uncertainty of 15% on the mass of the unactuated coordi-
882 nate (torso), that is

$$884 \quad m_{1u} = m_1 + \Delta m_1; \quad \Delta m_1 = 15\%$$

885 To see the effect of the introduced uncertainty on the
886 closed-loop system two figures are given. On Fig. 40 the

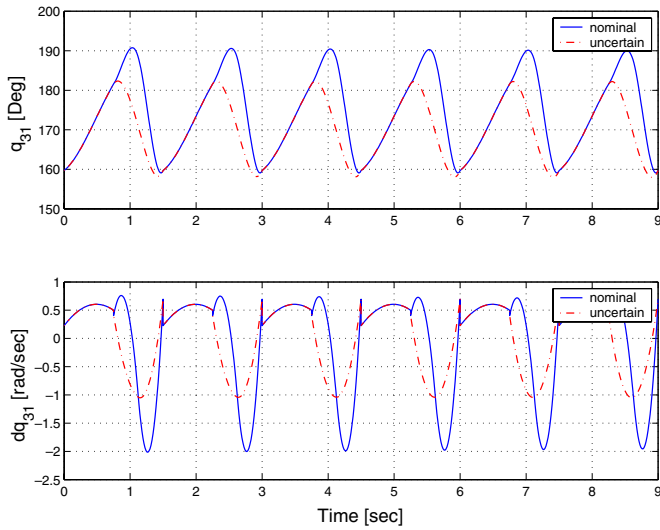


Fig. 34. (Sim 3) Position and velocity of the femur of the first leg.

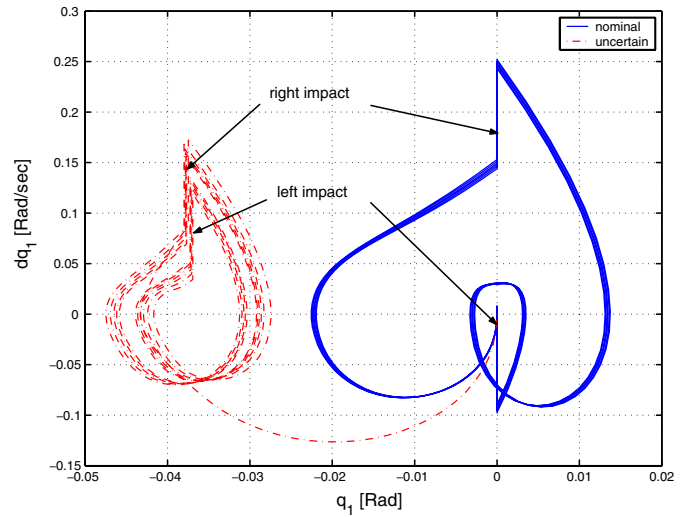


Fig. 37. (Sim 3) Phase portrait of the torso.

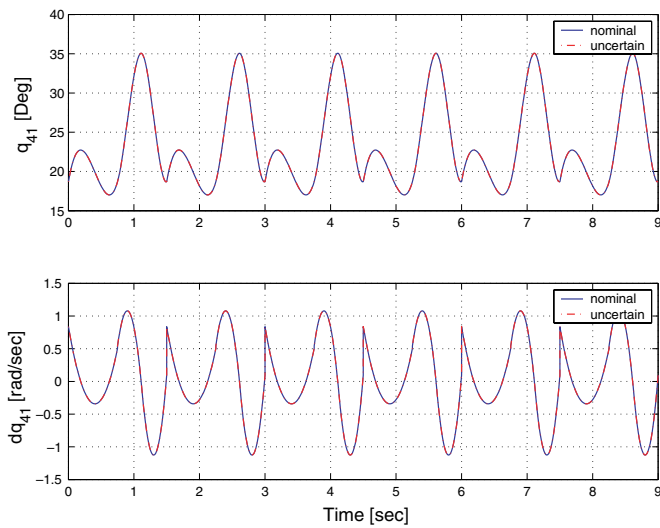


Fig. 35. (Sim 3) Position and velocity of the tibia of the first leg.

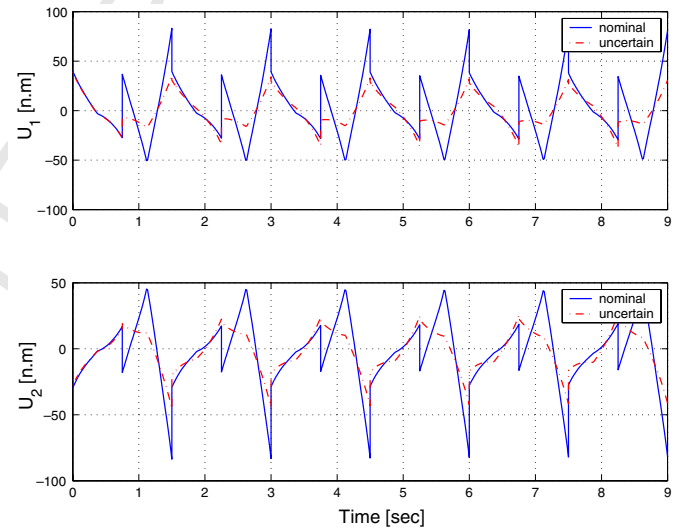


Fig. 38. (Sim 3) Torques of the femurs.

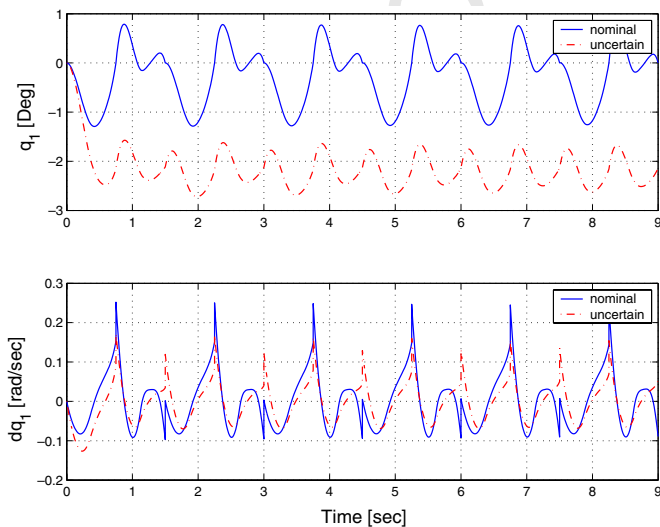


Fig. 36. (Sim 3) Position and velocity of the torso.

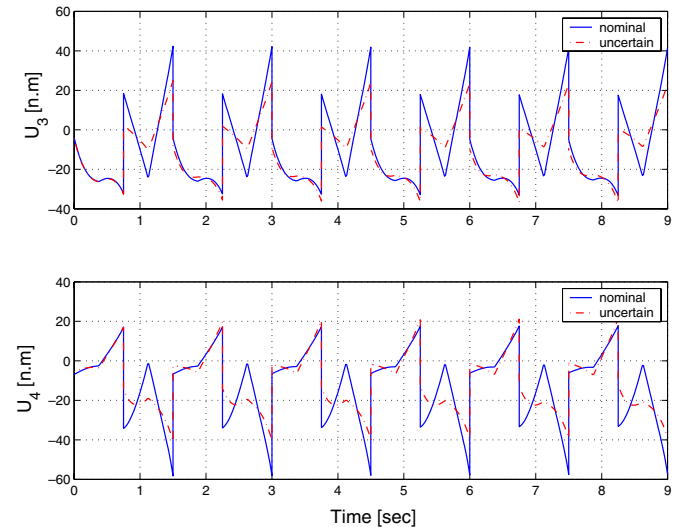


Fig. 39. (Sim 3) Torques of the tibias.

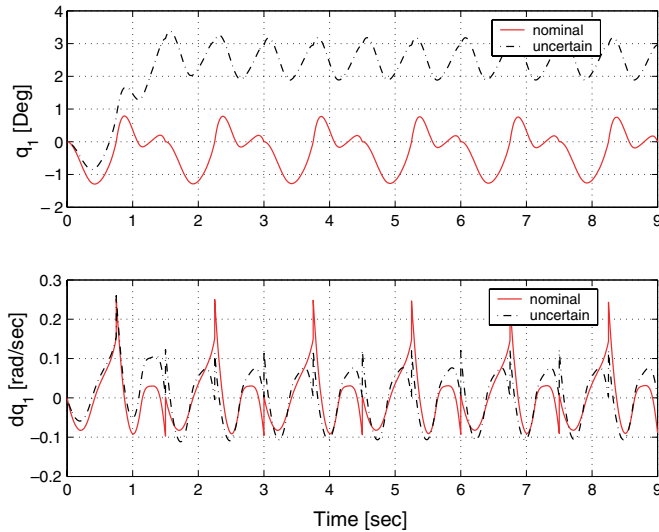


Fig. 40. (Sim 3) Position and velocity of the torso.

887 evolution of the position and the velocity of the torso are
 888 displayed. Where it could be seen clearly the convergence
 889 to a new cyclic trajectory for the uncertain system. An
 890 other interesting point result in the periodicity of the velocity
 891 trajectory which is of 1 cycle. This last fact could be bet-
 892 ter observed on Fig. 41 of the phase portrait, where one
 893 notices a convergence to an other stable limit cycle. How-
 894 ever the new limit cycle is of length 1, consequently the
 895 introduced uncertainty on the torso masse has induced a
 896 deformation of the limit cycle.

897 5.5. Simulation 4: robustness against ground irregularities

898 The aim is to investigate the robustness of the proposed
 899 controller, against ground irregularities. Let us make the
 900 robot walking on a horizontal surface with a stair at a dis-
 901 tance of 1.4 m from the robot, the stair is 1 cm height.

902 According to the robot configuration, namely the step
 903 length $d = 0.3$ m, the robot hits the stair during the fifth
 904 walking step.

905 The approach parameters are the same as previous simu-
 906 lations except the weighting matrix in the optimization
 907 criterion which is chosen $Q = \text{Diag}\{1, 0.1\}$, and the step
 908 duration which is of $t_f = 1$ s now. This change in these
 909 two parameters have been adopted because it gives a better
 910 results, namely a configuration with these parameters
 911 choice is more robust than the configuration with the old
 912 values.

913 The corresponding simulation results are depicted in
 914 Figs. 42–47. It is worth to note that the impact is detected
 915 at the instants $t = 1$ s for all steps, except for the step dur-
 916 ing which it hits the stair (fifth step), where the impact
 917 instant corresponding to this last one is $t = 0.935$ s, which
 918 is before the expected time $t = 1$ s.

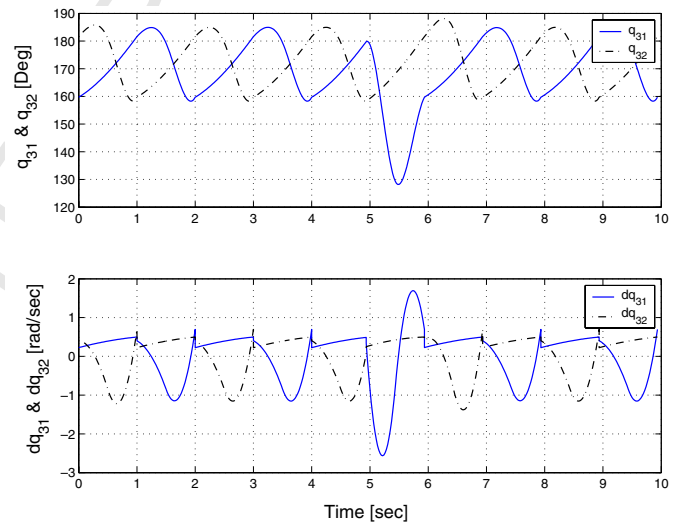


Fig. 42. (Sim 4) Position and velocity of the robot femurs.

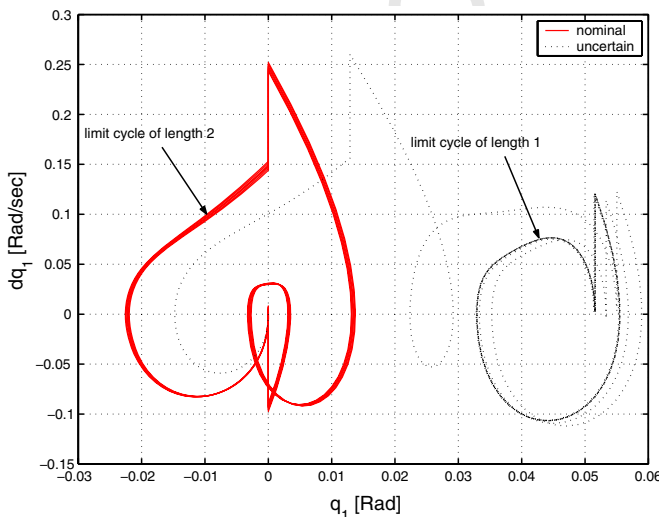


Fig. 41. (Sim 3) Phase portrait of the torso.

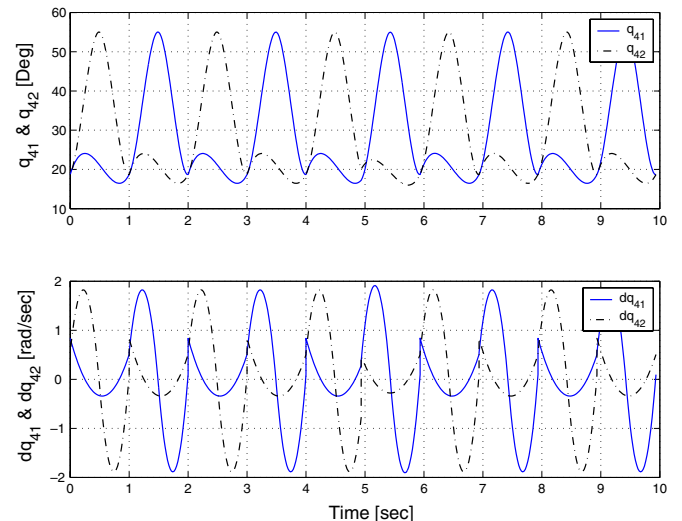


Fig. 43. (Sim 4) Position and velocity of the robot tibias.

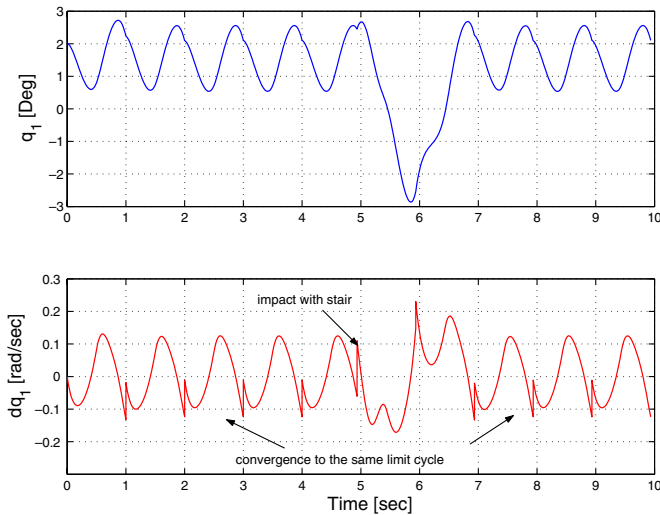


Fig. 44. (Sim 4) Position and velocity of the torso.

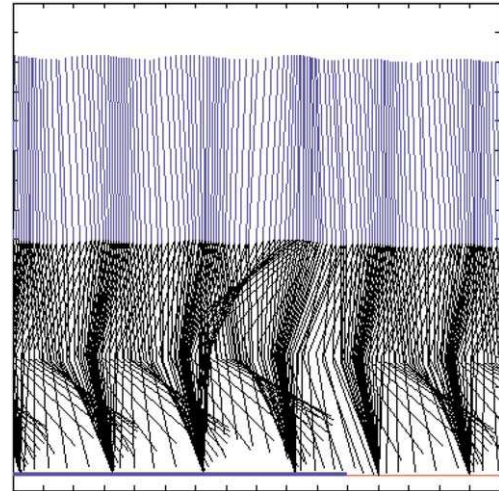


Fig. 47. (Sim 4) Stick figures of stair climbing.

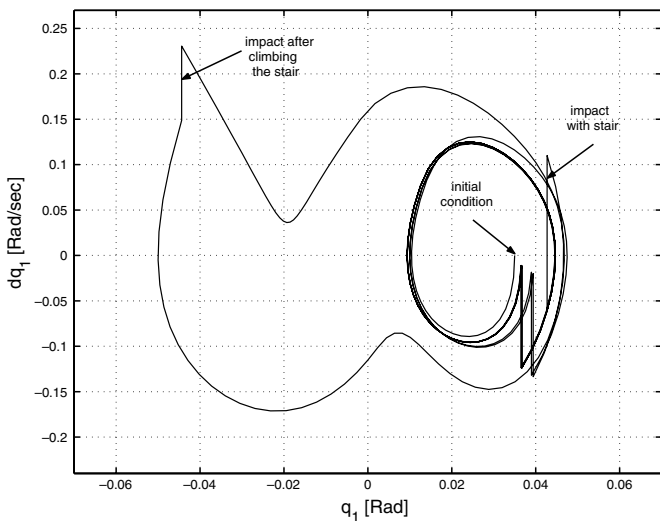


Fig. 45. (Sim 4) The phase portrait of the torso.

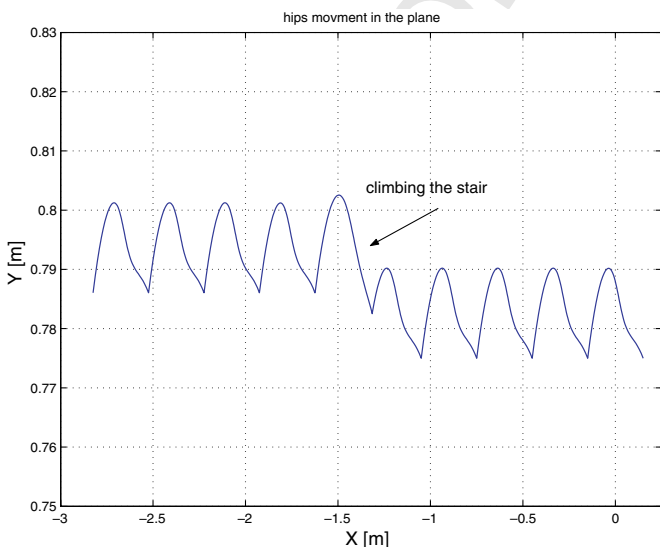


Fig. 46. (Sim 4) The hips trajectory in the sagittal plane.

Figs. 42 and 43 display the positions and velocities of the 919
 actuated robot's limbs versus time. The effect of the unex- 920
 pected impact could be seen on Fig. 42 as a removal from 921
 the cyclic trajectory followed by a convergence to the same 922
 trajectory. This effect can also be observed on the behavior 923
 of the unactuated coordinate (torso). Especially Fig. 44 924
 which shows the evolution of the angular position and 925
 velocity of the torso, and Fig. 45 which displays its phase 926
 portrait. On both figures a removal from the cyclic trajec- 927
 tory is observed, followed by a convergence to the same 928
 trajectory. It is worth to note that the limit cycle is of 929
 length 1 for this simulation. Fig. 46 depicts the hips trajec- 930
 tory in the sagittal plane, whereas Fig. 47 illustrates 931
 through a stick figures of the robot postures the climbing 932
 of the stair. 933

The limit of stair height beyond it the robot falls is closely 934
 related to the chosen configuration. For the actual configura- 935
 tion the limit is of 5 cm. Nevertheless this limit could be 936
 increased by changing the configuration, or the approach 937
 parameters. 938

6. Conclusion and future work 939

In this paper, a nonlinear low dimensional predictive 940
 control approach is proposed for the control of RABBIT, a 941
 walking five-link, seven d.o.f. under-actuated biped robot. 942
 The basic idea of the approach is to split up the vector of 943
 coordinates into actuated and unactuated variables. Then 944
 on-line optimization is used to update reference trajectories 945
 on the actuated coordinates, to aim to enhance the behavior 946
 as well as the stability of the unactuated variables. 947

The stability analysis of the resulting closed-loop system 948
 is carried out using a graphical tool based on the Poincaré 949
 section. Sufficient conditions for the stability of the motion 950
 are proposed and a concrete computation procedure is 951
 given to estimate the corresponding region of attraction 952
 related to the zero-dynamics of the closed-loop system. 953
 The particular case of scalar predictive control is success- 954

955 fully investigated by simulation and a reasonable regions of
956 attraction are obtained.

957 The resulting feedback seems to be real-time implement-
958 able thanks to the low dimension of the optimization
959 problem.

960 The whole framework is illustrated through simulation
961 case studies. Indeed four simulations are proposed. In the
962 first one walking at constant average speed starting from
963 rest is investigated, while the second scenario concerns
964 switching between different walking speeds. Robustness
965 of the proposed nonlinear predictive based-upon controller
966 is verified through the two last applications. In the first one
967 a robot model including parameters uncertainties (namely
968 uncertainties on inertias and masses) is considered, while
969 in the second, ground irregularities are considered. In spite
970 of these both significant disturbances the controller is able
971 to guide the robot suitably for walking while keeping it sta-
972 ble (no slipping, no falling).

973 In simulations, after each impact the reference trajecto-
974 ries on actuated coordinates are computed based on a pre-
975 defined step frequency. These trajectories are tracked while
976 checking at each decision instant if there is impact (RABBIT
977 prototype is equipped with switches at feet used to detect
978 impacts). If an impact is detected, the two legs are re-
979 labelled, the configuration of the robot is measured and a
980 new step starts up.

981 Future works may include other features, that should be
982 deeply investigated. In particular, one may be able to
983 choose the design parameters t_f , z_2^f and Q in order to opti-
984 mize some desired feature (mean energy, torque, robust-
985 ness). However, the key future work is naturally the
986 experimentations. This is currently in progress.

987 References

- 988 [1] Azevedo C, Poinet P. Commande prédictive pour la marche d'un
989 robot bipède sous actionné. In: CIFA 2002, 2002. p. 605–10.
- 990 [2] Berns K. Walking machine catalogue. Available from: http://gate1.fzi.de/ids/public_html/index2.htm, 2004.
- 991 [3] Brogliato B. Nonsmooth impact mechanics. Models, dynamics and
992 control. LNCIS, vol. 220. Springer Verlag; 1996.
- 993 [4] Camacho EF, Bordons C. Model predictive control. LNCIS. Sprin-
994 ger Verlag; 2004.
- 995 [5] Chaillet N, Abba G, Ostertag E. Double dynamic modelling and
996 computed torque control of a biped robot. In: Proceedings of IEEE/
997 RSJ international conference on intelligence robotics systems, p.
998 1149–53, Munich, Germany, 1994.
- 1000 [6] Chang T, Hurmuzlu Y. Sliding control without reaching phase and its
1001 application to bipedal locomotion. *J Dyn Syst Measure Contr*
1002 1993;115:447–55.
- 1003 [7] Chemori A, Loria A. Control of a planar under-actuated biped on a
1004 complete walking cycle. *IEEE Trans Automat Contr* 2004;49(5).
- 1005 [8] Chevallereau C. Parameterized control for under-actuated biped
1006 robots. In: IFAC World Congress, Barcelona, Spain, 2002.
- 1007 [9] Chevallereau C, Aoustin Y. Optimal reference trajectories for walking
1008 and running biped robot. *Robotica* 2001;19(5):557–69.
- 1009 [10] Chevallereau C, Abba G, Aoustin Y, Plestan F, Westervelt ER,
1010 Canudas de Wit C, et al. Rabbit: a testbed for advanced control
1011 theory. *IEEE Contr Syst Mag* 2003;23(5):57–79.
- [11] Fontes FACC. A general framework to design stabilizing nonlinear
model predictive controllers. *Syst Control Lett* 2001;42(2):127–43.
- [12] Grizzle JW, Abba G, Plestan F. Asymptotically stable walking for
biped robots: analysis via systems with impulse effects. *IEEE Trans
Automat Contr* 2001;46(1):51–64.
- [13] Gubina F, Hemami H, McGee RB. On the dynamic stability of biped
locomotion. *IEEE Trans Biomed Eng* 1974;21(12):102–8.
- [14] Hardt M, Kreutz-Delgado K, Helton J. Minimal energy control of a
biped robot with numerical methods and a recursive symbolic
dynamic model. In: Proceedings of 37th IEEE conference on decision
contr., Florida, USA, 1998. p. 413–16.
- [15] Hurmuzlu Y, Marghitu DB. Rigid body collisions of planar
kinematic chains with multiple contact points. *Int J Rob Res*
1994;13(1):82–92.
- [16] Katoh R, Mori M. Control method of biped locomotion giving
asymptotic stability of trajectory. *Automatica* 1984;20(4):405–14.
- [17] Khalil H. Nonlinear systems. Second Edition. Upper Saddle
River: Prentice Hall; 1996.
- [18] Kun A, Miller W. Adaptive dynamic balance of an experimental
biped robot. In: Proceedings of IEEE conference on robotics
automatics, 1996.
- [19] Magdalena L, Monasterio-Huelin F. A fuzzy logic controller with
learning through the evolution of its knowledge base. *Int J Approx
Reason* 1997;16(3/4):335–58.
- [20] Mayne DQ, Rawlings JB, Rao CV, Scokaert PO. Constrained model
predictive control: stability and optimality. *Automatica*
2000;36:789–814.
- [21] McGeer T. Passive dynamic walking. *Int J Robot Res*
1990;9(2):62–82.
- [22] Miura H, Shimoyama I. Dynamic walk of a biped. *Int J Rob Res*
1984;3(2):60–74.
- [23] Mrečki A, Waldron K. Human and machine locomotion.
LNCIS. Udine, Italy: Springer Verlag; 1997.
- [24] Nicholls E. Bipedal dynamic walking in robotics. Honours thesis,
University of western Australia, 1998.
- [25] Park JH. Impedance control for biped robot locomotion. *IEEE Trans
Robot Automat* 2001;17(6):870–82.
- [26] Plestan F. Commande de la marche d'un bipède type rabbit avec
trajectoires optimales et évaluation de la robustesse. In: CIFA 2002,
2002. p. 516–21.
- [27] Plestan F, Grizzle JW, Westervelt ER, Abba G. Stable walking of a 7
dof biped robot. *IEEE Trans Robot Automat* 2003;19(4):653–68.
- [28] Pratt J, Pratt G. Intuitive control of a planar bipedal walking robot.
In: Proceedings of IEEE Conference on Robotics Automat. Leuven,
Belgium, 1998. p. 2014–21.
- [29] Raibert MH. Legged robots. *Commun ACM* 1986;29:499–514.
- [30] Rostami M, Bessonnet G. Impactless sagittal gait of a biped robot
during the single support phase. In: Proceedings of the IEEE
Conference on Robotics Automat. Leuven, Belgium, 1998. p. 1385–
91.
- [31] Roussel L, Canudas C, Goswami A. Generation of energy optimal
complete gait cycles for biped robots. In: Proceedings of the IEEE
Conference on Robotics Automat. Leuven, Belgium, 1998. p. 2036–
41.
- [32] Sciavicco L, Siciliano B. Modeling and control of robot manipula-
tors. New York: McGraw Hill; 1996.
- [33] Spong M. Passivity based control of the compass gait biped. In:
IFAC World Congress, Beijing, China, 1999.
- [34] Westervelt ER. Towards a coherent framework for the control of
planar biped locomotion. PhD thesis, University of Michigan, 2003.
- [35] Westervelt ER, Grizzle JW, Canudas de Wit C. Switching and pi
control of walking motions of planar biped walkers. *IEEE Trans
Automat Contr* 2003;48(2):308–12.
- [36] Westervelt ER, Grizzle JW, Koditschek DE. Hybrid zero dynamics of
planar biped walkers. *IEEE Trans Automat Contr* 2003;48(1):42–56.